# CD27 is required for protective lytic EBV antigen specific CD8$^+$ T cell expansion

Yun Deng[1], Bithi Chatterjee[1], Kyra Zens[1,2], Hana Zdimerova[1], Anne Müller[1], Patrick Schumachers[1], Laure-Anne Ligeon[1], Antonino Bongiovanni[3,4], Riccarda Capaul[5], Andrea Zbinden[5], Angelika Holler[6], Hans Stauss[6], Wolfgang Hammerschmidt[7] and Christian Münz[1*]

[1]Viral Immunobiology, Institute of Experimental Immunology, University of Zurich, Switzerland.

[2]Institute of Epidemiology, Biostatistics and Prevention, University of Zurich, Switzerland.

[3]Cellular Microbiology of Infectious Pathogens Group, Center for Infection and Immunity of Lille, Institut Pasteur de Lille, Lille, France.

[4]BioImaging Center Lille-Nord de France, IFR142, Institut Pasteur de Lille, Lille, France.

[5]Institute of Medical Virology, University of Zurich, Switzerland.

[6]Institute of Immunity and Transplantation, Royal Free Campus, University College London, UK.

[7]Research Unit Gene Vectors, Helmholtz Zentrum München, German Research Center for Environmental Health and German Center for Infection Research, Germany.

Running title: CD27 mediated immune control of EBV

## KEY POINTS

- Blockade of CD27/CD70 interaction compromises EBV-specific immune control.
- CD27 is particularly required for the expansion and effector function of lytic EBV antigen specific $CD8^+$ T cells.

**ABSTRACT**

Primary immunodeficiencies in the co-stimulatory molecule CD27 and its ligand CD70 predispose for pathologies of uncontrolled Epstein Barr virus (EBV) infection in nearly all affected patients. We demonstrate that both depletion of CD27 positive cells and antibody blocking of CD27 interaction with CD70 causes uncontrolled EBV infection in mice with reconstituted human immune system components. While overall $CD8^+$ T cell expansion and composition is unaltered after antibody blocking of CD27, only some EBV specific $CD8^+$ T cell responses, exemplified by early lytic EBV antigen BMLF1 specific $CD8^+$ T cells are inhibited in their proliferation and killing of EBV transformed B cells. This suggests that CD27 is not required for all $CD8^+$ T cell expansions and cytotoxicity, but for a subset of $CD8^+$ T cell responses that protect us from EBV infection.

Keywords: CD27; CD70; humanized mice; Epstein Barr virus; cytotoxicity

## INTRODUCTION

Epstein Barr virus (EBV) is a common γ-herpesvirus that infects more than 95% of the human population [1]. At the same time, it was the first human tumor virus discovered in the 1960s [2,3]. It is also associated with a spectrum of pathologies in humans [4,5], ranging from B cell lymphomas and epithelial cell carcinomas to immunopathologies like hemophagocytic lymphohistiocytosis (HLH) and infectious mononucleosis (IM). The diverse manifestations of EBV pathology are connected to the lytic and 4 latent (latency 0 to III) gene expression programs that EBV can switch between in healthy virus carriers [6]. These are also mirrored in EBV associated malignancies, such as Burkitt's lymphoma (latency I) and Hodgkin's lymphoma (latency II). Despite this high pathogenic potential and wide distribution of EBV in the human populations the respective tumors are with an annual incidence of around 200'000, fortunately, quite rare [7].

A nearly perfect cell-mediated immune control protects us from EBV associated pathologies. This becomes apparent under conditions of primary or acquired immunodeficiencies, such as HIV co-infection [5,8,9]. They identify cytotoxic lymphocytes, mainly $CD8^+$ T cells, as the primary immune compartment for EBV specific immune control [10-12]. Defects in T cell receptor signalling have been identified in primary immunodeficiencies that predispose for EBV associated pathologies. These affect among others interleukin-2 inducible T cell kinase (ITK), ZAP70 and PI3K 110δ. Furthermore, development and expansion of cytotoxic lymphocytes is required for EBV specific immune control and this is compromised by mutations in GATA2, MCM4, XIAP, STK4 and CTPS1. The last group of molecules that are required for EBV associated immune control, affect co-stimulation of $CD8^+$ T cells. Among these, mutations in both CD27 and its ligand CD70 have been identified as a nearly exclusive cornerstone of EBV specific immune control. Previous research has shown that nearly all affected patients develop EBV associated pathologies, with HLH-like immunopathologies more often observed in CD27 deficiencies and Hodgkin's lymphoma more frequent in CD70 deficiencies [13-18].

Therefore, we investigated the requirement for CD27 positive lymphocytes and CD27 engagement of CD70 during EBV infection in mice with reconstituted human immune system components. We found that depletion of CD27 positive cells and blocking of CD27 compromised EBV specific immune control resulting in

elevated viral titres and expansion of infected $CD39^+CD70^+$ B cells. Overall $CD8^+$ T cell expansion was not compromised by CD27 blocking. However, the expansion and cytotoxicity of early lytic EBV antigen specific $CD8^+$ T cells, exemplified by BMLF1 specific cytotoxic lymphocytes, was abolished, suggesting that CD27 is required for an important part of the immune control of EBV.

## METHODS

### Humanized mouse generation and infection

NOD-scid $\gamma_c^{null}$ (NSG) mice and HLA-A2 transgenic NSG mice were maintained in ventilated, specific pathogen-free condition at the Institute of Experimental Immunology, University of Zurich. Newborn pups were reconstituted with human $CD34^+$ hematopoietic progenitor cells (HPCs). Mice with sufficient reconstitution of human immune cells were injected with $10^5$ Raji Green units (RGU) of EBV. The detailed procedure for NSG and NSG-A2 reconstitution and virus production are provided in the Supplemental Methods. All animal work strictly followed the animal protocols ZH209/2014 & ZH159/17, licensed by the veterinary office of the canton of Zurich, Switzerland.

### *In vivo* anti-CD27 antibody depletion and blocking

CD27 depleting mAB (clone: LG.3A10) and the corresponding Armenian hamster IgG isotype control (Biolegend) were injected i.p. at 12.5μg/g of the mouse weight two weeks post EBV infection and continued every 4 days until the termination of experiment. CD27 blocking mAB (clone: LG.3A10) and the corresponding mouse IgG1 isotype control (Absolute Antibody) were injected i.p. at 6.25μg/g of the mouse weight two weeks post EBV infection and continued every 4 days until the termination of experiment.

### ChipCytometry

Splenic tissues harvested at the termination of experiments were embedded in OCT (Tissue-Tek) at -80°C. Cryosections (5-6μm thick) were fixed and inserted into ZellSafe T chips (Canopy Biosciences) for staining. Samples labeled with fluorescent antibodies were acquired with a Zellkraftwerk ZellScanner One and its ZellExplorer software. After each round of acquisition, the fluorescent signals were photobleached and prepared for the next round of staining to accomplish a 27-marker panel. Additional details are provided in the Supplemental Methods.

### Laboratory assays

Multiple assays were conducted to analyse the experimental samples including flow cytometry, *in vivo* IVIS imaging, LCL generation, cytotoxicity assay,

immunohistochemistry and immunofluorescence, serum cytokine quantification and quantitative RT-PCR. Assay details are provided in the Supplemental Methods.

**Statistical analysis**

Statistical significance was calculated with 1) Mann-Whitney U test to analyze unpaired data with a non-Gaussian distribution, 2) one-way ANOVA (Kruskal-Wallis test) followed by Dunn's post hoc test or 3) two-way ANOVA with Sidak's (or Tukey's) multiple comparisons as post hoc test or 4) two-tailed unpaired t test by Prism 7 (GraphPad Software). D'Agostino-Pearson omnibus normality test was used to determine normality of data. All data points in the graphs are displayed with median and interquartile range, indicated with horizontal lines. N represents number of biological replicates unless otherwise stated. High-dimensional analysis details are provided in Supplemental Methods.

## RESULTS

### CD27 shows a similar expression pattern on T cells of humans and humanized mice.

To investigate the specific contribution of CD27 to EBV associated immune control, we have primarily used a mouse model with reconstituted human immune system compartments (humanized mice) that allows establishment of EBV infection, lymphomagenesis and its cell-mediated immune control *in vivo* [19,20] (Figure 1A). To examine whether humanized mice are a suitable model to study CD27 function, we characterized CD27 expression on single cell suspensions of peripheral blood mononuclear cells (PBMCs) of healthy donors and humanized mice. The majority of $CD27^+$ cells of both PBMC sources were $CD4^+$ and $CD8^+$ T cells (Figure S1A, Figure 1B). There was a similarly high level of expression on T cells in individual cell populations (Figure 1C). Slightly higher expression in the naïve population ($CCR7^+CD45RA^+$) but lower expression in Temra ($CCR7^-CD45RA^+$) and Tem ($CCR7^-CD45RA^-$) in $CD3^+CD27^+$ T cells was observed in humanized mice (Figures 1D and 1E). Taken together, these data demonstrate that CD27 has a similar distribution pattern on T cells in humanized mice and humans. Thus, we conclude that humanized mice are a suitable model to study the role of CD27 expression on human T cells for EBV infection.

### $CD27^+$ cells are important in the immune control of EBV viral loads and tumorigenesis during EBV infection in humanized mice

We next determined how important the $CD3^+CD27^+$ cells are to protect against EBV infection. To this end, we adopted the acute (or IM-like) EBV infection model by injecting humanized mice with $10^5$ Raji green unit (RGU) of B95-8 EBV [21]. In order to allow priming of EBV specific T cell responses prior to depletion, CD27 positive cells were depleted starting at week two post infection (Figure 2A). A depletion effect of $CD3^+CD27^+$ T cells was observed and persisted for up to six days (Figure S2A). Therefore, depleting antibody injection was repeated every four days. There was a significant drop in $CD3^+$ T cells in the peripheral blood under treatment (Figure 2B). A clear reduction in total $CD3^+$ T cell count was observed in both blood and spleen samples (Figures 2C and 2D). There was no significant difference in total $CD19^+$ B cell counts (Figure 2B), consistent with low CD27 expression in this immune compartment (Figure 1B and C). Loss of T cells in infected animals treated with

depleting antibody led to a higher frequency of tumor incidence (Figure 2E). Furthermore, EBV viral burden was significantly elevated in both blood and spleen after CD27 depletion (Figures 2F-H). The detected viral load is primarily cell-associated [22]. Consistently, the number of EBNA2-expressing cells, which indicates early virus-transformed B cells [23], was significantly increased in spleen (Figures 2I and 2J). Altogether, these experiments suggest an essential role of $CD27^+$ T cells in providing EBV specific immunity and preventing development of EBV associated malignancies.

**Blocking of CD27 diminishes the immune control of EBV infection**

We next sought to investigate the effect of CD27 co-stimulation on EBV-specific immune control using HLA-A2 transgenic humanized mice reconstituted with HLA-$A2^+$ $CD34^+$ HPCs (NSG-A2). To monitor both bulk T cell subsets and EBV antigen specific $CD8^+$ T cell responses, we adoptively transferred recombinant HLA-A2 restricted T cell receptor (TCR) transduced human T cells, previously isolated from donor-mate NSG-A2 animals, which are specific for either 1) the early lytic EBV antigen BMLF1 or 2) the latent EBV antigen LMP2 (Figures 3A and 3B). Both the TCR transduced (both specificities) and bulk $CD8^+$ T cells showed similar levels of CD27 expression before transfer (Figure 3B). Following transfer, humanized NSG-A2 mice were infected with luciferase-expressing EBV (Luc-EBV) in order to monitor the localization of infection by *in vivo* imaging and then treated with either CD27 blocking antibody or isotype control starting from week 2 after infection. There was no depletion effect on $CD3^+$ T and $CD19^+$ B cells observed (Figures S3A and S3B). The blocking effect of the antibody was checked by flow cytometry using two fluorochrome conjugated anti-CD27 antibodies (Figure S3C). While the antibody (clone: O323) derived from a different clone than the blocking antibody could still detect CD27 (Figure S3D), the antibody (clone: LG.3A10) derived from the same clone as the blocking antibody was inhibited from binding (Figure S3E).

Animals treated with CD27 blocking antibody exhibited splenomegaly 5 weeks post-infection (Figure 3C). However, CD27 blocking did not seem to have an effect on animal weight (Figure S3F) and survival (Figure S3G). A significant increase in blood viral loads was observed upon CD27 blocking (Figure 3D) as well as in spleen and liver (Figure 3E). Viral loads of the groups transferred with BMLF1 or LMP2 specific T cells or mock transduced cells were not different (Figures S3H).

Additionally, the number of EBNA2 positive cells was significantly higher in splenic sections upon CD27 blocking (Figures 3F and 3G) and CD27 expression on EBV infected B cells in blood and spleen was also higher (Figure S3I). To assess the viral burden and infection progression, mice were imaged with an IVIS Spectrum Imaging System on a weekly basis. The bioluminescent signal showed a significantly higher level due to CD27 blocking at week 5 post EBV infection (Figures 3H and 3I). Moreover, with respect to individual EBV gene expression, both latent genes (EBER1, EBNA2, LMP1, LMP2a and EBNA1_Wp) and lytic genes (BMLF1, BMRF1, BGLF5, BNLF2a and BILF1) were higher expressed after blocking CD27 (Figure S3J).

In order to examine if CD27 blocking has a selective effect on immune control of latent or lytic EBV infection, humanized NSG mice were infected with wild type EBV and compared with BZLF1 knock-out EBV (BZkoEBV) that cannot switch into lytic replication. Interestingly, wild type EBV infected animals showed significantly higher spleen weights (Figure 3J) and viral loads in both blood and spleen (Figures 3K and 3L) upon CD27 blocking, as compared to animals infected with BZkoEBV with and without CD27 inhibition. Additionally, the number of EBNA2 positive cells was significantly higher in wild type EBV infected animals treated with the anti-CD27 antibody, as compared to the other groups (Figures S3K and S3L). Taken together, these data reveal that CD27 blockade leads to loss of EBV specific immune control, primarily against lytic EBV antigen expression.

**$CD70^+CD39^+EBNA2^+$ B cells accumulate upon loss of CD27 mediated immune control of EBV**

To better understand which EBV infected B cells accumulate in the absence of CD27 mediated immune control, we checked their phenotype on sacrifice day (Figure 3A). It has been previously shown that expression of both CD70 and CD39 are up-regulated on lymphoblastoid cell lines (LCLs), which consist of EBV transformed B cells [24,25]. Both markers were reported to be highly expressed in B-cell lymphomas such as germinal center B-cell-like (GCB) and activated B-cell-like diffuse large B-cell lymphomas (DLBCL) [26,27]. We observed significantly increased expression of CD70 and CD39 in the peripheral blood, spleen and liver (Figures 4A-C) upon CD27 blocking. No significant increase was seen in $CD73^+$ and $CD39^+CD73^+$ populations (Figure 4B). However, CD39 frequency positively correlated with EBV viral loads

(Figure 4D). Additionally, we found reduced expression of CXCR5 and CCR7 after blocking CD27, two chemokine receptors important for B cell migration into lymphoid organs (Figures 4E and 4F).

Next, we assessed the co-expression of CD70 and CD39, together with Ki67 for B cell proliferation and EBNA2 for EBV infection in blood (Figure S4A) and spleen (Figure S4B). Two phenotypically distinct populations were identified with respect to the expression of CD70 and CD39 (Figures 4F and 4G). In animals treated with anti-CD27 blocking antibody, we found the $CD70^{+}CD39^{+}$ population was more expanded and showed high co-expression of Ki67 and EBNA2 in blood (Figure 4H). The same phenotypic difference was also observed in spleen (Figures S4C-4E). In summary, these results suggest that CD27 blocking allows accumulation of $CD39^{+}CD70^{+}$ DLBCL-like EBV infected B cells with possibly more aggressive proliferative behavior.

**Early EBV lytic antigen BMLF1 specific $CD8^{+}$ T cells require CD27 for expansion and cytotoxicity**

We next addressed whether CD27 blocking affected particularly EBV specific $CD8^{+}$ T cell responses *in vivo*. In line with CD27 deficient patient data, which showed normal T cell differentiation compared to healthy controls in peripheral blood [14], our results demonstrated that CD27 blockade did not lead to a change in bulk T cell differentiation (Figure 5A), as well as in the memory subset composition of EBV specific $CD8^{+}$ T cells (Figure S5A) in blood. No significant difference was also observed in spleen, liver and bone marrow (Figure S5B). We next examined BMLF1 and LMP2 specific $CD8^{+}$ T cells which were adoptively transferred into the animals (Figure 5B). In line with CD27 blocking mainly affecting immune control of lytic EBV infection, there was an impaired expansion of BMLF1 specific $CD8^{+}$ T cells in animals treated with CD27 blocking antibody longitudinally in blood (Figure 5C), while such a difference was not observed for LMP2 specific $CD8^{+}$ T cells (Figure 5D). Further analysis in spleen and liver showed similar results with selective impairment of BMLF1 specific, but not LMP2 specific $CD8^{+}$ T cells (Figures 5E and 5F). Moreover, significantly increased Ki67 expression on BMLF1 specific $CD8^{+}$ T cells (depicted as CD8 Pent+ cells), as compared to non-BMLF1 specific T cells (depicted as CD8 Pent- cells), was observed in the isotype antibody treated group. However, CD27 blockade seemed to suppress proliferation of BMLF1 specific $CD8^{+}$ T cells as

Ki67 expression was reduced comparable to bulk $CD8^+$ T cell levels (Figures 5G-5H). By contrast, LMP2 specific $CD8^+$ T cells showed no difference (Figure 5I).

Given that cytotoxicity is the main protective T cell function during EBV infection, we further assessed T cell cytolytic response by co-culturing LCLs with BMLF1 and LMP2 specific $CD8^+$ T cell clones, generated *ex vivo* from the autologous healthy human donor [28]. We found that BMLF1 specific T cells showed significantly reduced cytotoxic activity against LCLs after blocking CD27 at the effector to target ratio of 10 to 1 (Figures 5J and 5K). However, the proliferation of LCLs was not influenced by CD27 blocking (Figure S5B). In summary, these data reveal a differential susceptibility of early lytic and latent EBV antigen-specific $CD8^+$ T cells to CD27 blockade during EBV infection.

**CD27 blockade compromises $CXCR5^+EOMES^+$ $CD8^+$ T cell accumulation during EBV infection**

To interrogate the alterations in proinflammatory cytokine production after CD27 blockade, we examined terminal serum samples. Animals treated with the CD27 blocking antibody exhibited significantly elevated levels of IFNγ, IL-10 and highly increased levels of TNFα (Figure 6A), suggesting that CD27 blocking increases the inflammatory immune responses which might contribute to EBV associated pathologies. Consistent with a more proinflammatory environment, CD27 blockade also led to a moderately decreased expression of CXCR5 on $CD8^+$ T cells in blood and liver (Figure 6B).

We next assessed the differential expression of T-box transcription factors (T-bet) and eomesodermin (EOMES), which are key drivers for effector functions and long-term memory formation of T cells [29,30]. We found the frequency of $EOMES^{bright}$ $T\text{-}bet^{dim}$ $CD8^+$ T cells to be reduced after CD27 blockade (Figures 6C), indicating that cytotoxic effector and effector memory T cell functions are decreased. In addition, the expression of the activation/tissue residency marker CD69 was diminished (Figure 6D), whereas an upregulation in the expression of co-stimulatory 2B4 and inhibitory PD1 was observed on $CD8^+$ T cells (Figure 6E).

To obtain spatial information of activated $CD8^+$ T cells in relation to EBV infected B cells, we investigated splenic sections by ChipCytometry, a multiplexing tissue imaging technology that allows for repeated rounds of immunofluorescence

staining and bleaching to assess multiple parameters in histological sections. $CD20^+$ B cells and $CD8^+$ T cells were aggregated in white pulp areas of isotype control treated spleens (Figure S6A). We assessed a 27-marker panel plus a nuclear staining (Table S1, Figure S6C, D, E and F) by ChipCytometry and observed co-localization between CD20 and EBNA2, CD8 and CD69, and CD8 and PD1 in splenic white pulp areas (Figure 6F). Quantification of segmented cells showed higher frequencies of $CD8^+$ T cells and $EBNA2^+CD20^+$ cells after CD27 blockade (Figures S6B). The ratio of $CD8^+$/$EBNA2^+CD20^+$ cells was significantly higher upon CD27 blocking, suggesting compromised immune control despite efficient $CD8^+$ T cell expansion. However, $CD8^+$ T cells were similarly activated as judged by PD1 and CD69 expression (Figure 6G). Thus, these results suggested that CD27 blockade may compromise terminal cytotoxic $CD8^+$ T cell differentiation with homing capacity to germinal centers in secondary lymphoid organs, where cytotoxic EBV specific immune control needs to take place.

## DISCUSSION

In this study, we performed *in vivo* experiments using humanized mice as an EBV infection model to address CD27 deficiency during EBV specific immune responses. Both $CD27^+$ lymphocyte depletion and CD27 blocking compromised EBV specific immune control. We deciphered that CD27 blockade had a dramatic effect on the protective function of early lytic EBV antigen (BMLF1) specific $CD8^+$ T cells, but to a lesser extent on latent EBV antigen (LMP2) specific $CD8^+$ T cells, despite the elevated gene expression of BMLF1 in B cells of the CD27 blocking antibody treated group (Figure 3J), which should have driven BMLF1 specific T cell expansion more efficiently. In line with our findings, previous studies in CD27 deficient patients showed a detectable level of EBV specific T cells against LMP2 and autologous LCL restimulation [13,17], suggesting that CD27 signaling may be involved in expansion of early lytic antigen specific cytotoxic $CD8^+$ T cell responses. In line with these findings CD27 was required for the immune control of wild-type but not lytic replication deficient EBV infection.

Although CD27 has been reported to regulate T cell survival, expansion and memory generation [31-33], its blocking did not seem to have an impact on overall T cell differentiation during EBV infection in humanized mice. This is consistent with clinical observations from both CD27 and CD70 deficient patience [14,16,18], in which

the T cell repertoire composition seems also largely unaltered compared to healthy controls. Consistent with our findings, only some, but not other EBV specific $CD8^+$ T cell responses were diminished in the affected patients [16,18]. These CD27 dependent T cell specificities might be stimulated by and target early EBV infected B cells in which CD70 peaks at day 5 in mRNA and day 8 in protein expression after infection [34,35], and even earlier leaky lytic EBV antigen expression can be targeted by $CD8^+$ T cells to eliminate EBV infected B cells [36]. These data from both CD27 blocking in humanized mice and CD27 or CD70 deficient patients argue that absence of CD27/CD70 signaling does not alter T cell repertoire composition or even bulk $CD8^+$ T cell expansion to EBV infection, but that a subset of protective $CD8^+$ T cell responses against lytic EBV antigens, exemplified by BMLF1 specific $CD8^+$ T cells, depends on CD27 for their expansion and cytotoxicity.

Interestingly, patients with RASGRP1 deficiency, the main activator of the MAP kinase pathway, exhibited a reduced T cell expansion in a CD27 dependent manner [37]. RASGRP1 deficient T cells failed to proliferate upon stimulation with $CD70^{high}$ LCLs [37,38]. This result further confirmed the importance of CD27/CD70 and the downstream MAP kinase pathway in the expansion of EBV-specific T cells.

Other co-stimulatory molecules affecting T cell interactions with B cells also seem to play a unique role in immunity to EBV. For instance, it has been discovered that in X-linked lymphoproliferative disease type 1 (XLP-1) the deficiency of the SLAM-associated protein (SAP) compromises co-stimulatory 2B4 function [39]. This leads to a profound effect on cytotoxicity against EBV infected B cells [40,41], however, it still allows expansion of EBV specific $CD8^+$ T cells [42,43]. Accordingly, humanized mice present with similar $CD8^+$ T cell expansion but less controlled EBV infection after antibody blocking of 2B4, and SAP deficient patients suffer from EBV pathology despite their normal frequencies of EBV specific $CD8^+$ T cells [41,44]. This implies that 2B4 might only be required for cytotoxic $CD8^+$ T cell recognition of EBV transformed B cells, while CD27 promotes expansion and cytotoxicity of a subset of protective EBV specific $CD8^+$ T cells. Possibly compensatory 2B4 up-regulation was observed on $CD8^+$ T cells in our experiments upon CD27 blocking, but diminished expression of this co-receptor was reported in CD27 or CD70 deficient patients [18]. In contrast to the better understood role of CD27 and 2B4, the functions of 4-1BB, NKG2D, CTLA-4 and PD-1 that are required for EBV specific immune control still need to be defined [21,45-49]. However, different EBV associated

pathologies were observed in primary immunodeficiencies affecting these molecules suggest their non-redundant roles in controlling virus infection. A better understanding of these underlying mechanisms should allow us to harness these co-stimulatory and co-inhibitory functions for immune modulation.

The selective loss of expansion and cytotoxicity of a subset of EBV specific $CD8^+$ T cells was also associated with a significant up-regulation in the co-expression of CD39 and CD70 on the EBV infected B cells in our study. This indicates more activation of B cells after blocking CD27/CD70 interaction, which might promote EBV mediated growth transformation and development of persistent infection in B cells, ultimately resulting in DLBCL-like malignancies. This altered phenotype of EBV infected B cells might be the result of higher EBV viral loads or selective targeting of $CD39^+CD70^+$ EBV infected B cells by the CD27 dependent $CD8^+$ T cell response. However, in the absence of efficient cytotoxicity against B cells through the CD27/CD70 axis, elevated proinflammatory cytokines might also provoke higher expression of CD70 on EBV infected B cells. Similar results have also been reported for CD48, the ligand of 2B4, which was up-regulated in SAP deficiency during EBV infection [40]. Thus, not only overall EBV infection increases upon CD27 blocking, but also the phenotype of the infected B cells seems to change.

These $CD39^+$ B cells might be mainly involved in the expansion of BMLF1 specific $CD8^+$ T cells and in turn be controlled by the subset of EBV specific cytotoxic $CD8^+$ T cell responses that fail to expand during CD27 blocking and deficiency, indicating that this subset of EBV specific $CD8^+$ T cells are particularly sensitive to CD27 deficiency. In contrast, $CD8^+$ T cell responses to the related β-herpesvirus human cytomegalovirus (HCMV) that has with 50% also a high prevalence in the human population have been shown to be $CD27^-CD28^-$ [50]. This might at least explain why EBV, but not HCMV specific immune control by T cells is sensitive to CD27 or CD70 deficiency. The near exclusive susceptibility of CD27 or CD70 deficient patients to EBV pathology argues that most common infections apart from EBV follow the HCMV example.

Collectively, these results suggest a unique and non-redundant role of CD27 to EBV specific immunity, mainly emphasizing its function in T cell expansion and cytotoxicity, primarily of a subset of EBV specific T cells, such as BMLF1 specific $CD8^+$ T cells. Absence of immune control by these CD27 dependent $CD8^+$ T cells

leads to uncontrolled EBV infection. Our results also support a possibly protective role of early antigen specific $CD8^+$ T cell responses against EBV infection and lymphomagenesis [1]. Moreover, restoration of the CD27/CD70 pathway by CD27 agonistic antibody could be a therapeutic approach for the treatment of EBV associated lymphomas, especially in patients with a CD70 deficiency.

## ACKNOWLEDGMENTS

The authors thank all members of the Core Facility of the UZH including the Cytometry Facility and the Center for Microscopy and Image Analysis for assistance, and the Laboratory Animal Services Center (LASC) for animal husbandry.

## AUTHORSHIP CONTRIBUTIONS

Contribution: Y.D. designed the study, performed the majority of the experiments and analysed the data. B.C., K.Z., and H.Z. helped with design and perform experiments; A.M., L.-A.L. and A.B. performed the ChipCyometry and its quantification; P.S., R.C. and A.Z. established the quantification of viral loads; A.H. and H.S. generated the TCR constructs; W.H. provided with the Luc-EBV and C.M. designed the study with Y.D. and supervised the study; Y.D. and C.M. prepared the figures and wrote the manuscript.

Conflict-of-interest disclosure: HJS is a founder of Quell Therapeutics, shareholder of Quell Therapeutics and shareholder of Kuur Therapeutics. All other authors declare no competing financial interests.

Correspondence: Christian Münz, Institute of Experimental Immunology, University of Zurich, Winterthurerstrasse 190, CH-8057 Zurich, Switzerland; e-mail: muenzc@immunology.uzh.ch

## REFERENCES

1. Münz C. Latency and lytic replication in the oncogenesis of the Epstein Barr virus. *Nat Rev Micobiol*. 2019;17:691-700.

2. Epstein MA, Achong BG, Barr YM. Virus particles in cultured lymphoblasts from Burkitt's lymphoma. *Lancet*. 1964;1:702-703.

3. Epstein MA, Henle G, Achong BG, Barr YM. Morphological and biological studies on a virus in cultured lymphoblasts from Burkitt's lymphoma. *J Exp Med*. 1964;121:761-770.

4. Taylor GS, Long HM, Brooks JM, Rickinson AB, Hislop AD. The immunology of Epstein-Barr virus-induced disease. *Annu Rev Immunol*. 2015;33:787-821.

5. Shannon-Lowe C, Rickinson A. The Global Landscape of EBV-Associated Tumors. *Front Oncol*. 2019;9:713.

6. Babcock GJ, Thorley-Lawson DA. Tonsillar memory B cells, latently infected with Epstein-Barr virus, express the restricted pattern of latent genes previously found only in Epstein-Barr virus-associated tumors. *Proc Natl Acad Sci U S A*. 2000;97(22):12250-12255.

7. Cohen JI, Fauci AS, Varmus H, Nabel GJ. Epstein-Barr virus: an important vaccine target for cancer prevention. *Sci Transl Med*. 2011;3(107):107fs107.

8. Totonchy J, Cesarman E. Does persistent HIV replication explain continued lymphoma incidence in the era of effective antiretroviral therapy? *Curr Opin Virol*. 2016;20:71-77.

9. McHugh D, Myburgh R, Caduff N, et al. EBV renders B cells susceptible to HIV-1 in humanized mice. *Life Sci Alliance*. 2020;3(8):e202000640.

10. Latour S, Fischer A. Signaling pathways involved in the T-cell-mediated immunity against Epstein-Barr virus: Lessons from genetic diseases. *Immunol Rev*. 2019;291(1):174-189.

11. Damania B, Münz C. Immunodeficiencies that predispose to pathologies by human oncogenic gamma-herpesviruses. *FEMS Microbiol Rev*. 2019;43:181-192.

12. Tangye SG, Latour S. Primary immunodeficiencies reveal the molecular requirements for effective host defense against EBV infection. *Blood*. 2020;135(9):644-655.

13. Salzer E, Daschkey S, Choo S, et al. Combined immunodeficiency with life-threatening EBV-associated lymphoproliferative disorder in patients lacking functional CD27. *Haematologica*. 2013;98(3):473-478.

14. van Montfrans JM, Hoepelman AI, Otto S, et al. CD27 deficiency is associated with combined immunodeficiency and persistent symptomatic EBV viremia. *J Allergy Clin Immunol*. 2012;129(3):787-793 e786.

15. Alkhairy OK, Perez-Becker R, Driessen GJ, et al. Novel mutations in TNFRSF7/CD27: Clinical, immunologic, and genetic characterization of human CD27 deficiency. *J Allergy Clin Immunol*. 2015;136(3):703-712 e710.

16. Abolhassani H, Edwards ES, Ikinciogullari A, et al. Combined immunodeficiency and Epstein-Barr virus-induced B cell malignancy in humans with inherited CD70 deficiency. *J Exp Med*. 2017;214(1):91-106.

17. Izawa K, Martin E, Soudais C, et al. Inherited CD70 deficiency in humans reveals a critical role for the CD70-CD27 pathway in immunity to Epstein-Barr virus infection. *J Exp Med*. 2017;214(1):73-89.

18. Ghosh S, Kostel Bal S, Edwards ESJ, et al. Extended clinical and immunological phenotype and transplant outcome in CD27 and CD70 deficiency. *Blood*. 2020.

19. Münz C. Humanized mouse models for Epstein Barr virus infection. *Curr Opin Virol*. 2017;25:113-118.

20. McHugh D, Caduff N, Murer A, et al. Infection and immune control of human oncogenic gamma-herpesviruses in humanized mice. *Philos Trans R Soc Lond B Biol Sci*. 2019;374(1773):20180296.

21. Chatterjee B, Deng Y, Holler A, et al. $CD8^+$ T cells retain protective functions despite sustained inhibitory receptor expression during Epstein-Barr virus infection in vivo. *PLoS Pathog*. 2019;15:e1007748.

22. Chijioke O, Muller A, Feederle R, et al. Human natural killer cells prevent infectious mononucleosis features by targeting lytic Epstein-Barr virus infection. *Cell Rep*. 2013;5(6):1489-1498.

23. Rabson M, Gradoville L, Heston L, Miller G. Non-immortalizing P3J-HR-1 Epstein-Barr virus: a deletion mutant of its transforming parent, Jijoye. *J Virol*. 1982;44(3):834-844.

24. Rowe M, Rowe DT, Gregory CD, et al. Differences in B cell growth phenotype reflect novel patterns of Epstein-Barr virus latent gene expression in Burkitt's lymphoma cells. *Embo J*. 1987;6(9):2743-2751.

25. Young LS, Rickinson AB. Epstein-Barr virus: 40 years on. *Nat Rev Cancer*. 2004;4(10):757-768.

26. Bertrand P, Maingonnat C, Penther D, et al. The costimulatory molecule CD70 is regulated by distinct molecular mechanisms and is associated with overall survival in diffuse large B-cell lymphoma. *Genes Chromosomes Cancer*. 2013;52(8):764-774.

27. Cardoso CC, Auat M, Santos-Pirath IM, et al. The importance of CD39, CD43, CD81, and CD95 expression for differentiating B cell lymphoma by flow cytometry. *Cytometry B Clin Cytom*. 2018;94(3):451-458.

28. Antsiferova O, Müller A, Rämer P, et al. Adoptive transfer of EBV specific $CD8^+$ T cell clones can transiently control EBV infection in humanized mice. *PLoS Pathog*. 2014;10(8):e1004333.

29. Knox JJ, Cosma GL, Betts MR, McLane LM. Characterization of T-bet and eomes in peripheral human immune cells. *Front Immunol*. 2014;5:217.

30. Paley MA, Kroy DC, Odorizzi PM, et al. Progenitor and terminal subsets of $CD8^+$ T cells cooperate to contain chronic viral infection. *Science*. 2012;338(6111):1220-1225.

31. de Jong R, Loenen WA, Brouwer M, et al. Regulation of expression of CD27, a T cell-specific member of a novel family of membrane receptors. *J Immunol*. 1991;146(8):2488-2494.

32. Jung J, Choe J, Li L, Choi YS. Regulation of CD27 expression in the course of germinal center B cell differentiation: the pivotal role of IL-10. *Eur J Immunol*. 2000;30(8):2437-2443.

33. van Lier RA, Borst J, Vroom TM, et al. Tissue distribution and biochemical and functional properties of Tp55 (CD27), a novel T cell differentiation antigen. *J Immunol*. 1987;139(5):1589-1596.

34. Pich D, Mrozek-Gorska P, Bouvet M, et al. First Days in the Life of Naive Human B Lymphocytes Infected with Epstein-Barr Virus. *MBio*. 2019;10(5).

35. Mrozek-Gorska P, Buschle A, Pich D, et al. Epstein-Barr virus reprograms human B lymphocytes immediately in the prelatent phase of infection. *Proc Natl Acad Sci U S A*. 2019;116(32):16046-16055.

36. Brooks JM, Long HM, Tierney RJ, et al. Early T Cell Recognition of B Cells following Epstein-Barr Virus Infection: Identifying Potential Targets for Prophylactic Vaccination. *PLoS Pathog*. 2016;12(4):e1005549.

37. Winter S, Martin E, Boutboul D, et al. Loss of RASGRP1 in humans impairs T-cell expansion leading to Epstein-Barr virus susceptibility. *EMBO Mol Med*. 2018;10(2):188-199.

38. Roose JP, Mollenauer M, Gupta VA, Stone J, Weiss A. A diacylglycerol-protein kinase C-RasGRP1 pathway directs Ras activation upon antigen receptor stimulation of T cells. *Mol Cell Biol*. 2005;25(11):4426-4441.

39. Cannons JL, Tangye SG, Schwartzberg PL. SLAM family receptors and SAP adaptors in immunity. *Annu Rev Immunol*. 2011;29:665-705.

40. Hislop AD, Palendira U, Leese AM, et al. Impaired Epstein-Barr virus-specific $CD8^+$ T-cell function in X-linked lymphoproliferative disease is restricted to SLAM family-positive B-cell targets. *Blood*. 2010;116(17):3249-3257.

41. Latour S, Winter S. Inherited Immunodeficiencies With High Predisposition to Epstein-Barr Virus-Driven Lymphoproliferative Diseases. *Front Immunol*. 2018;9:1103.

42. Parolini S, Bottino C, Falco M, et al. X-linked lymphoproliferative disease. 2B4 molecules displaying inhibitory rather than activating function are responsible for the inability of natural killer cells to kill Epstein-Barr virus-infected cells. *J Exp Med*. 2000;192(3):337-346.

43. Tangye SG. XLP: clinical features and molecular etiology due to mutations in SH2D1A encoding SAP. *J Clin Immunol*. 2014;34(7):772-779.

44. Chijioke O, Marcenaro E, Moretta A, Capaul R, Münz C. The SAP-dependent 2B4 receptor mediates $CD8^+$ T cell dependent immune control of Epstein Barr virus infection in mice with reconstituted human immune system components. *J Infect Dis*. 2015;212(5):803-807.

45. Alosaimi MF, Hoenig M, Jaber F, et al. Immunodeficiency and EBV-induced lymphoproliferation caused by 4-1BB deficiency. *J Allergy Clin Immunol*. 2019;144(2):574-583 e575.

46. Chaigne-Delalande B, Li FY, O'Connor GM, et al. Mg2+ regulates cytotoxic functions of NK and CD8 T cells in chronic EBV infection through NKG2D. *Science*. 2013;341(6142):186-191.

47. Johnson DB, McDonnell WJ, Gonzalez-Ericsson PI, et al. A case report of clonal EBV-like memory CD4(+) T cell activation in fatal checkpoint inhibitor-induced encephalitis. *Nat Med*. 2019;25(8):1243-1250.

48. Schwab C, Gabrysch A, Olbrich P, et al. Phenotype, penetrance, and treatment of 133 CTLA-4-insufficient individuals. *J Allergy Clin Immunol*. 2018.

49. Volk V, Theobald SJ, Danisch S, et al. PD-1 Blockade Aggravates Epstein-Barr Virus$^{+}$ Post-Transplant Lymphoproliferative Disorder in Humanized Mice Resulting in Central Nervous System Involvement and CD4$^{+}$ T Cell Dysregulations. *Front Oncol*. 2020;10:614876.

50. Appay V, Dunbar PR, Callan M, et al. Memory CD8$^{+}$ T cells vary in differentiation phenotype in different persistent virus infections. *Nat Med*. 2002;8(4):379-385.

## FIGURE LEGENDS

**Figure 1. Comparison of CD27 expression between immune cell populations of humans and humanized mice**

(A) Humanized mice (huMice) reconstitution scheme. Immunodeficient NOD mice with a loss-of-function mutation in the *Prkdc* gene and common γ chain deficiency (NOD-scid $\gamma_c^{null}$, NSG) were engrafted with human $CD34^+$ hematopoietic progenitor cells (HPCs) to reconstitute human immune system components and were tested for human immune compartment reconstitution after three months.

(B) Pie charts show the distribution of $CD27^+$ cells in different immune cell populations examined in huMice blood (n=3) and human PBMCs (n=3).

(C) Frequency of $CD27^+$ cells in different immune cell populations, comparing huMice peripheral blood (n=3) and human PBMCs (n=3).

(D-E) Representative flow cytometry analysis illustrating the gating strategy to differentiate memory T cell subsets characterized by CCR7 and CD45RA expression within the $CD3^+CD27^+$ population (D) and the frequency of each subset (E), comparing huMice peripheral blood (n=3) and human PBMCs (n=3). See also related Figure S1.

**Figure 2. $CD27^+$ cells are essential for the immune control of EBV viral loads and tumorigenesis during EBV infection**

(A) Workflow of CD27 depletion experiments. HuMice mice were infected (i.p.) with $10^5$ Raji Green Units (RGU) of B95-8 EBV. At week 2 post EBV infection, animals were injected (i.p.) with 12.5μg/g of either anti-CD27 depletion antibody or isotype control antibody consecutively every 4 days to ensure the depletion effect until termination of experiment.

(B-E) Frequency of $CD3^+$ T cells in anti-CD27 depleting antibody treated group (α-CD27 depl.) and isotype control antibody treated group (IsoCtrl. depl.) (B), frequency of $CD3^+$ T cells at the termination of experiment (C), total $CD3^+$ T cell count (D) and tumor burden in the respective groups (E).

(F-H) EBV viral loads quantified by qPCR over time (F), and at termination of experiment in peripheral blood (G) and spleen (H). The lower limit of quantification (LLOQ) of 122 IU/ml is depicted as horizontal dashed line.

(I-J) Immunohistochemistry images of EBNA2 in the respective groups, original magnification 200x (I), and the quantification of $EBNA2^+$ cells/$mm^2$ in splenic sections (J). Images are representative from one of two independent experiments.
Data (n=8-13 per group) are pooled from two independent mouse experiments in graph (B-H) and (J) and displayed with median and interquartile range. Two-way ANOVA analysis and Sidak's multiple comparisons as a post hoc test was used for (B), (E) and (F), Mann-Whitney test was used for (C-H) and (J) to assess p values; **p<0.01, ***p<0.001, ****p<0.0001. See also related Figure S2.

**Figure 3. Blocking of CD27 diminishes the immune control of EBV infection**

(A) Workflow of CD27 blocking experiments. One day before infection with $10^5$ Raji Green Units (RGU) of luciferase encoding B95-8 EBV (Luc-EBV), huNSG-A2 mice (HLA-A2 transgenic NSG mice reconstituted with HLA-$A2^+$ human hematopoietic progenitor cells) were adoptively transferred (AT) with 200'000 autologous T cells expressing either BMLF1 or LMP2 specific TCRs that had been transduced *ex vivo*. The anti-CD27 blocking antibody is the Fc domain re-engineered version of the anti-CD27 depletion antibody of Figure 2 and can no longer engage antibody directed cellular cytotoxicity (ADCC). At week 1 post EBV infection, animals were injected (i.p.) with 6.5µg/g of either anti-CD27 blocking antibody or isotype control antibody consecutively every 4 days until termination of experiment.
(B) Representative flow cytometry plots of BMLF1- and LMP2-specific TCR transduced $CD8^+$ T cells (left) using mouse TCRβ specific antibodies (mTCRb) and BMLF1 and LMP2 peptide plus HLA-A2 pentamers [26]. Frequency of CD27 expression on transduced and non-transduced $CD8^+$ T cells (right).
(C) Spleen weight of animals treated with either anti-CD27 blocking antibody (α-CD27 blo.) or isotype control antibody (IsoCtrl. blo.) upon different transfer conditions.
(D-E) EBV viral loads quantified by qPCR over time during EBV infection (D), at the termination of experiment in peripheral blood (E, left), spleen (E, middle) and liver (E, right). Mice treated with either anti-CD27 blocking antibody or isotype control antibody in different transfer conditions were compared.

(F-G) Representative immunohistochemistry images of EBNA2 in the respective groups, original magnification 200x (F), and the quantification of $EBNA2^+$ cells/$mm^2$ in splenic sections (G).
(H-I) Representative IVIS image analysis at week 1 and week 5 post Luc-EBV infection (H) and quantification of defined region of interest (ROI) of IVIS images (I).
(J) Spleen weight of animals infected with either wild type EBV or BZLF1 knock-out EBV (BZkoEBV), treated with anti-CD27 blocking antibody or isotype control antibody without adoptive transfer.
(K-L) EBV viral loads of animals over time during EBV infection (K), at the termination of experiment in peripheral blood (L, left) and spleen (L, right) in the respective groups.
Data (n= 14-16 per group) are pooled from two independent mouse experiments in graphs (C-E), (G) and (I-L) and displayed with median and interquartile range. Graphs (F-I) (n= 7-8 per group) are representative from one out of two independent experiments. Graphs (K-L) (n=4-6 per group) are from one experiment. One-way ANOVA analysis (Kruskal-Wallis test) followed by Tukey's post hoc test was used for (J) and (L). Two-way ANOVA analysis and Sidak's multiple comparisons as a post hoc test was used for (D), (I) and (K), and Mann-Whitney test for (C), (E) and (G) to assess p values; *$p<0.05$, **$p<0.01$. See also related Figure S3.

**Figure 4. $CD70^+CD39^+EBNA2^+$ B cells accumulate upon loss of CD27 mediated immune control of EBV**

(A) Frequency of CD70 expression on $CD19^+$ B cells in multiple organs (blood, spleen and liver) in anti-CD27 blocking antibody versus isotype control antibody treated group.
(B) Flow cytometry plots of CD39 and CD73 expression on $CD19^+$ B cells in multiple organs (blood, spleen and liver) in the indicated experimental groups.
(C) Frequency of CD39 expression on $CD19^+$ B cells.
(D) Correlation between the CD39 expression on $CD19^+$ B cells and EBV viral loads in blood.
(E) Frequency of CXCR5 expression on $CD19^+$ B cells.
(F) Representative UMAP analysis depicts clusters with co-expression of CD39, CD70, Ki67 and EBNA2 on $CD19^+$ B cells in blood.

(G) Data from (F) were transformed and shown in percentile of each population in anti-CD27 blocking antibody versus isotype control antibody treated group.
(H) Representative heatmap analysis of co-expression of CD39, CD70, Ki67 and EBNA2 on $CD19^+$ B cells in blood.
Data (n= 14-16 per group) are pooled from two independent mouse experiments in graph (A) and (C-E) and displayed with median and interquartile range. Graphs (F-H) (n= 7-8 per group) are representative from one of two independent experiments. Mann-Whitney test was used for (A), (C) and (E) to assess p values; Spearman correlation examining rank correlation was used for D. *p<0.05, **p<0.01, ***p<0.001. See also related Figure S4.

**Figure 5. Early EBV lytic antigen BMLF1 specific $CD8^+$ T cells require CD27 for expansion and cytotoxicity**

(A) $CD8^+$ T cell memory subsets characterized by CD45RA and CD62L expression and depicted as naïve, Tcm, Tem and Temra in groups treated with either anti-CD27 blocking antibody or isotype control antibody *in vivo*.
(B) Weekly representative flow cytometry plots showing the gating strategy and circulating BMLF1 and LMP2 specific $CD8^+$ T cells in blood *in vivo*.
(C-D) Longitudinal data examining the expansion of BMLF1 (C) and LMP2 (D) specific $CD8^+$ T cells in blood over time post Luc-EBV infection, treated with anti-CD27 blocking antibody versus isotype control antibody.
(E-F) Frequency of BMLF1 (E) and LMP2 (F) specific $CD8^+$ T cells in multiple organs (blood, spleen and liver) at termination of experiment.
(G) Representative flow cytometry plot of EBV specific TCR transduced $CD8^+$ T cells (depicted as CD8 $Pent^+$) and the rest of the T cells (depicted as CD8 $Pent^-$) using mouse TCRβ specific antibodies (mTCRb) and either BMLF1 or LMP2 peptide plus HLA-A2 pentamers [26].
(H-I) Frequency of Ki67 expressing cells showing the cell proliferation of EBV specific BMLF1 (H) and LMP2 (I) specific $CD8^+$ T cells (depicted as CD8 $Pent^+$ cells) versus the rest of $CD8^+$ T cells (depicted as CD8 $Pent^-$ cells) in blood in different experimental groups.
(J-K) *In vitro* killing assay with BMLF1 and LMP2 specific T cell clones generated from healthy EBV carriers *ex vivo*. T cells were pre-treated with either anti-CD27

blocking antibody or isotype control antibody and co-cultured with PHK-26 pre-labeled autologous LCLs for 21h at the indicated effector-to-target ratios (J), and at the ratio of 10:1 (K).

Data (n= 5-6 per group) are pooled from two independent mouse experiments in graph (A) and (C-I) and displayed with median and interquartile range. Two-way ANOVA analysis and Sidak's multiple comparisons as a post hoc test was used for (C) and (D) and Mann-Whitney test for (A) and (E-I). Data shown in (J-K) are pooled from three experiments and analyzed using two-tailed unpaired t test, dashed line signifies target cell only. (p values; *p<0.05, **p<0.01, ns: not significant)

See also related Figure S5.

**Figure 6. CD27 blockade compromises CXCR5$^+$EOMES$^+$ CD8$^+$ T cell accumulation during EBV infection**

(A) Cytokine production from serum samples harvested at termination of experiment. Each individual cytokine is presented in the separate transfer conditions in the upper panel. In the lower panel, pooled data of α-CD27 blocking antibody treated or isotype control antibody treated groups is shown.

(B) Frequency of CXCR5 expression on CD8$^+$ T cells in the respective groups in blood, spleen and liver.

(C) Frequency of EOMES bright T-bet dim and EOMES dim T-bet bright populations in the respective group in blood.

(D) Frequency of CD69 expression on CD8$^+$ T cells in spleen.

(E) Frequency of 2B4 (left) and PD1 (right) expression on CD8$^+$ T cells in Spleen.

(F) Representative ChipCytometry immunofluorescence images for CD20, EBNA2, CD8, CD69 and PD1 in splenic sections of the respective treatment groups. Scale bars are 50μm.

(G) Quantification of the CD8$^+$/EBNA2$^+$CD20$^+$ ratio, as well as the frequency of CD8$^+$CD69$^+$ and CD8$^+$PD1$^+$ cells in 5 to 7 randomly selected fields in splenic sections of isotype control or CD27 blocking antibody treated animals.

Data (n= 14-16 per group) are pooled from two independent mouse experiments in graphs (A), (B) and (D-F) and displayed with median and interquartile range. Mann-Whitney test for was used for (A), (B) and (D-F) and (G) to assess p values; *p<0.05, **p<0.01, ***p<0.001.

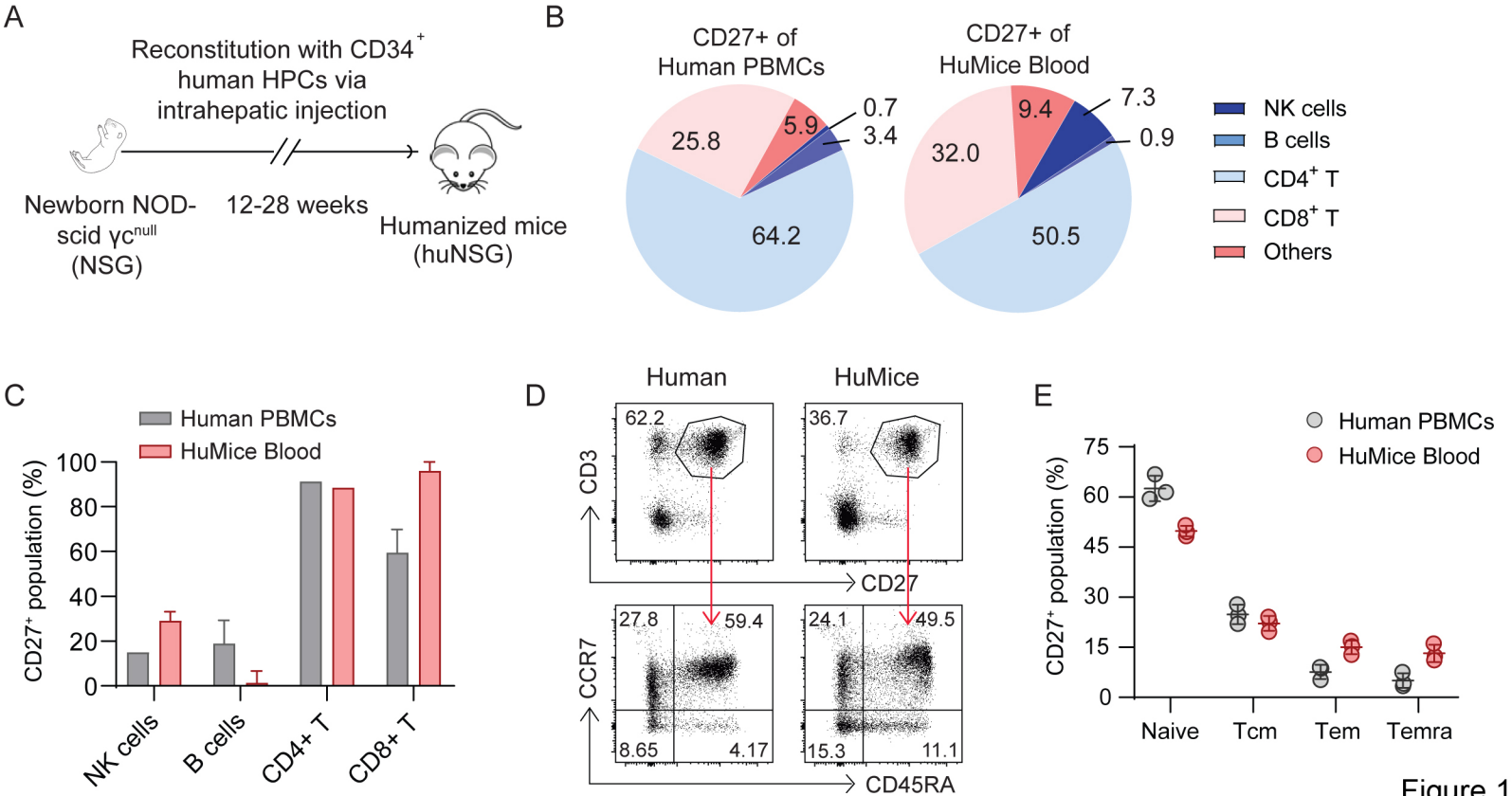
A
Reconstitution with CD34+ human HPCs via intrahepatic injection
Newborn NOD-scid γc^null (NSG)
12-28 weeks
Humanized mice (huNSG)
B
CD27+ of Human PBMCs
25.8
5.9
0.7
3.4
64.2
CD27+ of HuMice Blood
32.0
9.4
7.3
0.9
50.5
NK cells
B cells
CD4+ T
CD8+ T
Others
C
Human PBMCs
HuMice Blood
CD27+ population (%)
100
80
60
40
20
0
NK cells
B cells
CD4+ T
CD8+ T
D
Human
HuMice
CD3
CD27
62.2
36.7
CCR7
CD45RA
27.8
59.4
8.65
4.17
24.1
49.5
15.3
11.1
E
Human PBMCs
HuMice Blood
CD27+ population (%)
75
60
45
30
15
0
Naive
Tcm
Tem
Temra

Figure 1

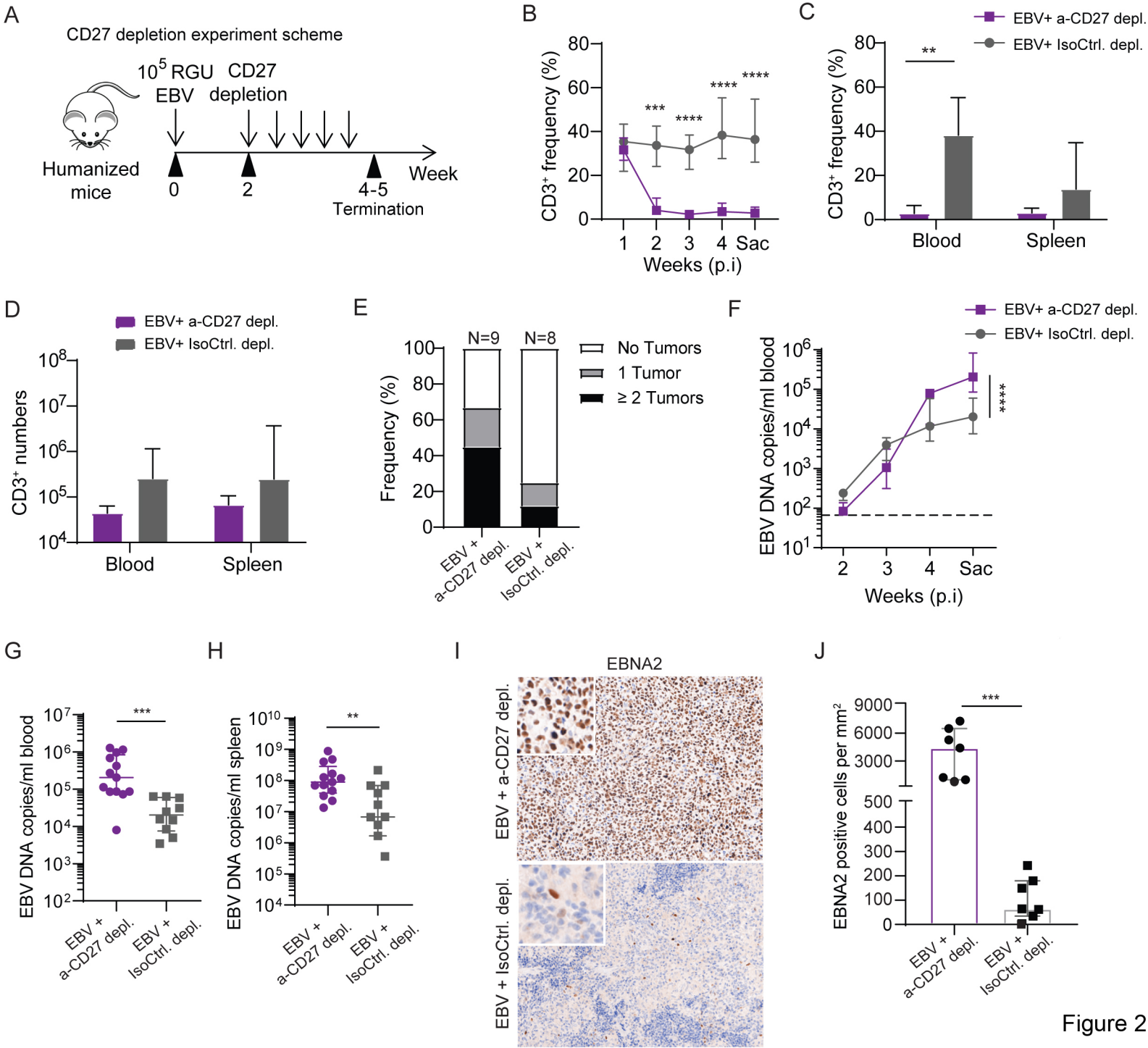
A
CD27 depletion experiment scheme
10^5 RGU EBV
CD27 depletion
Humanized mice
0
2
4-5 Termination
Week
B
CD3+ frequency (%)
Weeks (p.i)
1 2 3 4 Sac
***
****
****
****
C
EBV+ a-CD27 depl.
EBV+ IsoCtrl. depl.
CD3+ frequency (%)
**
Blood
Spleen
D
EBV+ a-CD27 depl.
EBV+ IsoCtrl. depl.
CD3+ numbers
Blood
Spleen
E
N=9
N=8
No Tumors
1 Tumor
≥ 2 Tumors
Frequency (%)
EBV + a-CD27 depl.
EBV + IsoCtrl. depl.
F
EBV+ a-CD27 depl.
EBV+ IsoCtrl. depl.
EBV DNA copies/ml blood
****
Weeks (p.i)
2 3 4 Sac
G
EBV DNA copies/ml blood
***
EBV + a-CD27 depl.
EBV + IsoCtrl. depl.
H
EBV DNA copies/ml spleen
**
EBV + a-CD27 depl.
EBV + IsoCtrl. depl.
I
EBNA2
EBV + a-CD27 depl.
EBV + IsoCtrl. depl.
J
EBNA2 positive cells per mm2
***
EBV + a-CD27 depl.
EBV + IsoCtrl. depl.

Figure 2

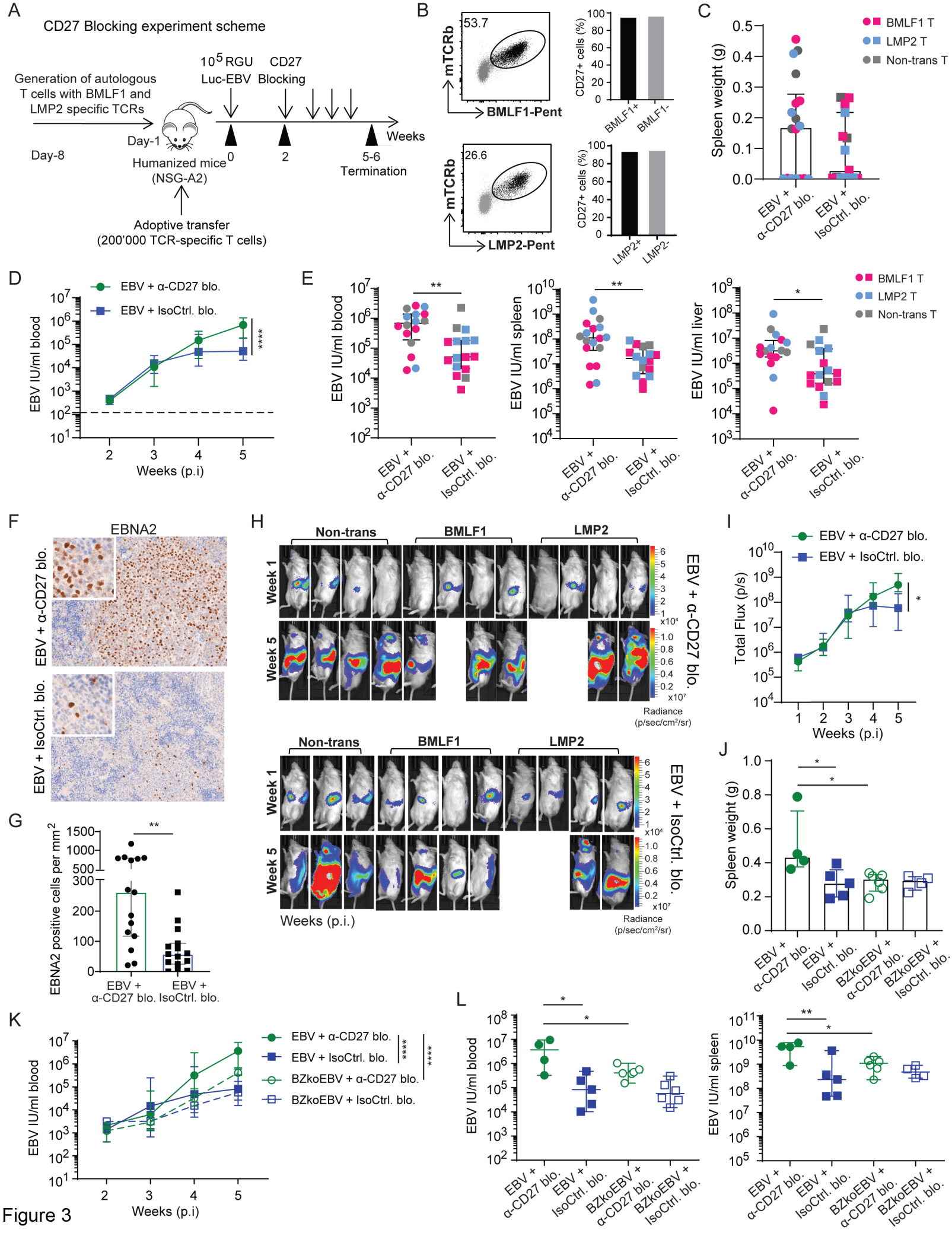
A
CD27 Blocking experiment scheme
Generation of autologous T cells with BMLF1 and LMP2 specific TCRs
Day-8
Day-1
Humanized mice (NSG-A2)
Adoptive transfer (200'000 TCR-specific T cells)
10^5 RGU Luc-EBV
CD27 Blocking
0
2
5-6 Termination
Weeks
B
53.7
mTCRb
BMLF1-Pent
CD27+ cells (%)
BMLF1+
BMLF1-
26.6
LMP2-Pent
LMP2+
LMP2-
C
BMLF1 T
LMP2 T
Non-trans T
Spleen weight (g)
EBV + α-CD27 blo.
EBV + IsoCtrl. blo.
D
EBV IU/ml blood
Weeks (p.i)
E
EBV IU/ml spleen
EBV IU/ml liver
F
EBNA2
G
EBNA2 positive cells per mm2
H
Non-trans
BMLF1
LMP2
Week 1
Week 5
Radiance (p/sec/cm²/sr)
Weeks (p.i.)
I
Total Flux (p/s)
J
BZkoEBV + α-CD27 blo.
BZkoEBV + IsoCtrl. blo.
K
L

Figure 3

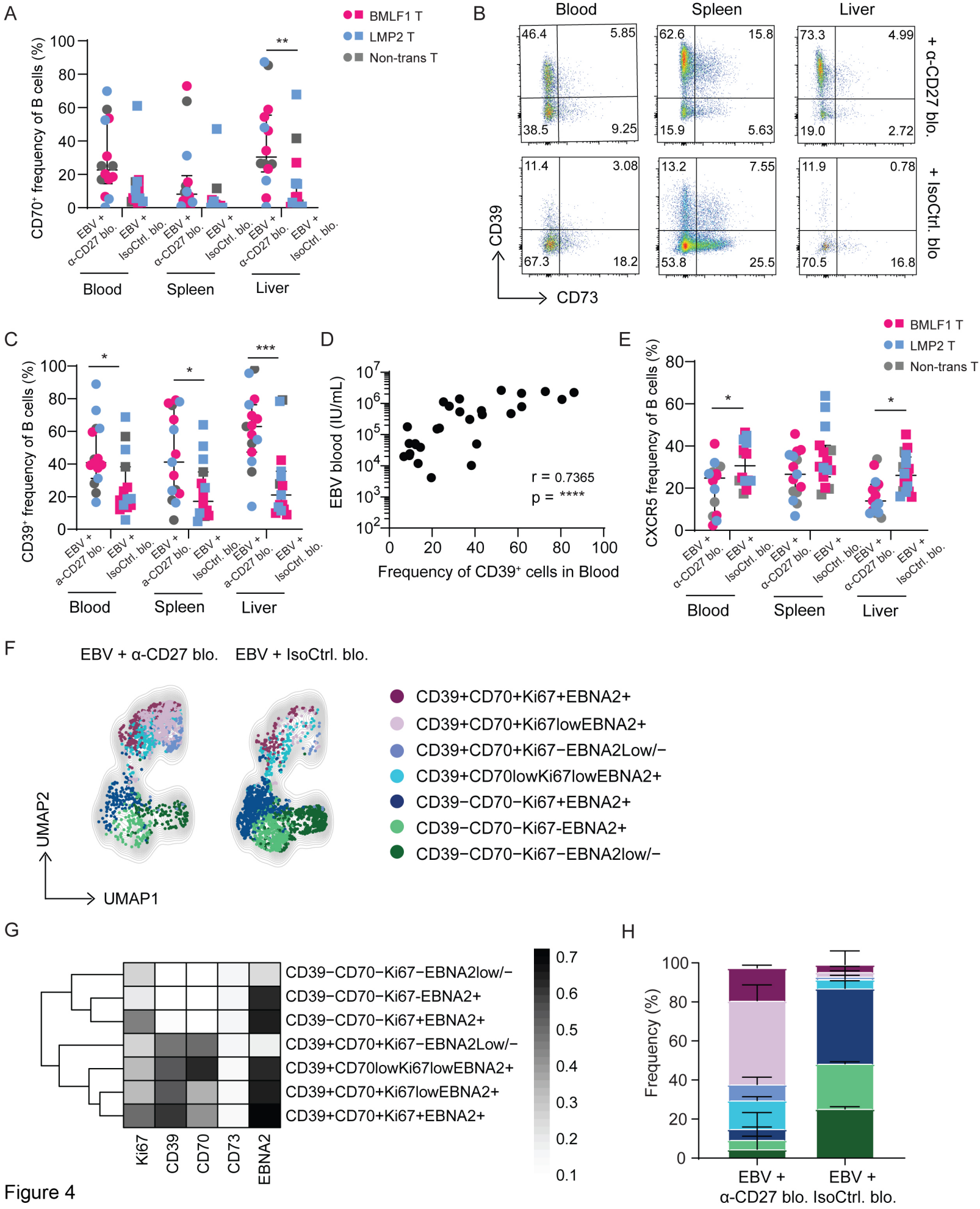
A
BMLF1 T
LMP2 T
Non-trans T
CD70⁺ frequency of B cells (%)
EBV + α-CD27 blo.
EBV + IsoCtrl. blo.
Blood
Spleen
Liver
B
Blood
Spleen
Liver
+ α-CD27 blo.
+ IsoCtrl. blo
CD39
CD73
C
CD39⁺ frequency of B cells (%)
D
EBV blood (IU/mL)
r = 0.7365
p = ****
Frequency of CD39⁺ cells in Blood
E
CXCR5 frequency of B cells (%)
F
EBV + α-CD27 blo.
EBV + IsoCtrl. blo.
UMAP2
UMAP1
CD39+CD70+Ki67+EBNA2+
CD39+CD70+Ki67lowEBNA2+
CD39+CD70+Ki67−EBNA2Low/−
CD39+CD70lowKi67lowEBNA2+
CD39−CD70−Ki67+EBNA2+
CD39−CD70−Ki67-EBNA2+
CD39−CD70−Ki67−EBNA2low/−
G
Ki67
CD39
CD70
CD73
EBNA2
H
Frequency (%)
EBV + α-CD27 blo.
EBV + IsoCtrl. blo.

Figure 4

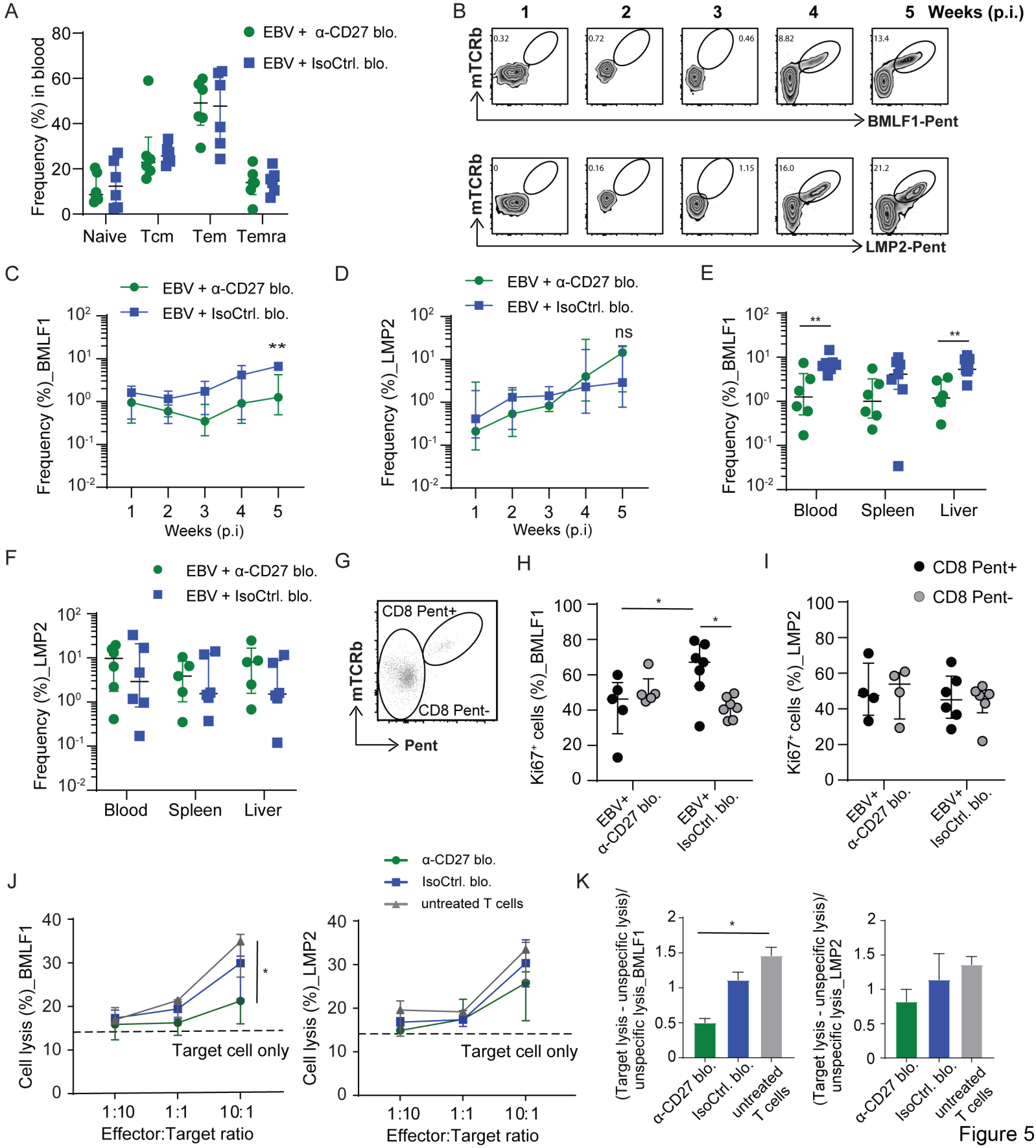
A
EBV + α-CD27 blo.
EBV + IsoCtrl. blo.
Frequency (%) in blood
Naive
Tcm
Tem
Temra
B
1
2
3
4
5 Weeks (p.i.)
mTCRb
BMLF1-Pent
LMP2-Pent
C
Frequency (%)_BMLF1
Weeks (p.i)
**
D
Frequency (%)_LMP2
ns
E
Blood
Spleen
Liver
F
G
CD8 Pent+
CD8 Pent-
Pent
H
Ki67+ cells (%)_BMLF1
I
Ki67+ cells (%)_LMP2
J
α-CD27 blo.
IsoCtrl. blo.
untreated T cells
Cell lysis (%)_BMLF1
Cell lysis (%)_LMP2
Target cell only
Effector:Target ratio
K
(Target lysis - unspecific lysis)/ unspecific lysis_BMLF1
(Target lysis - unspecific lysis)/ unspecific lysis_LMP2
untreated T cells

Figure 5

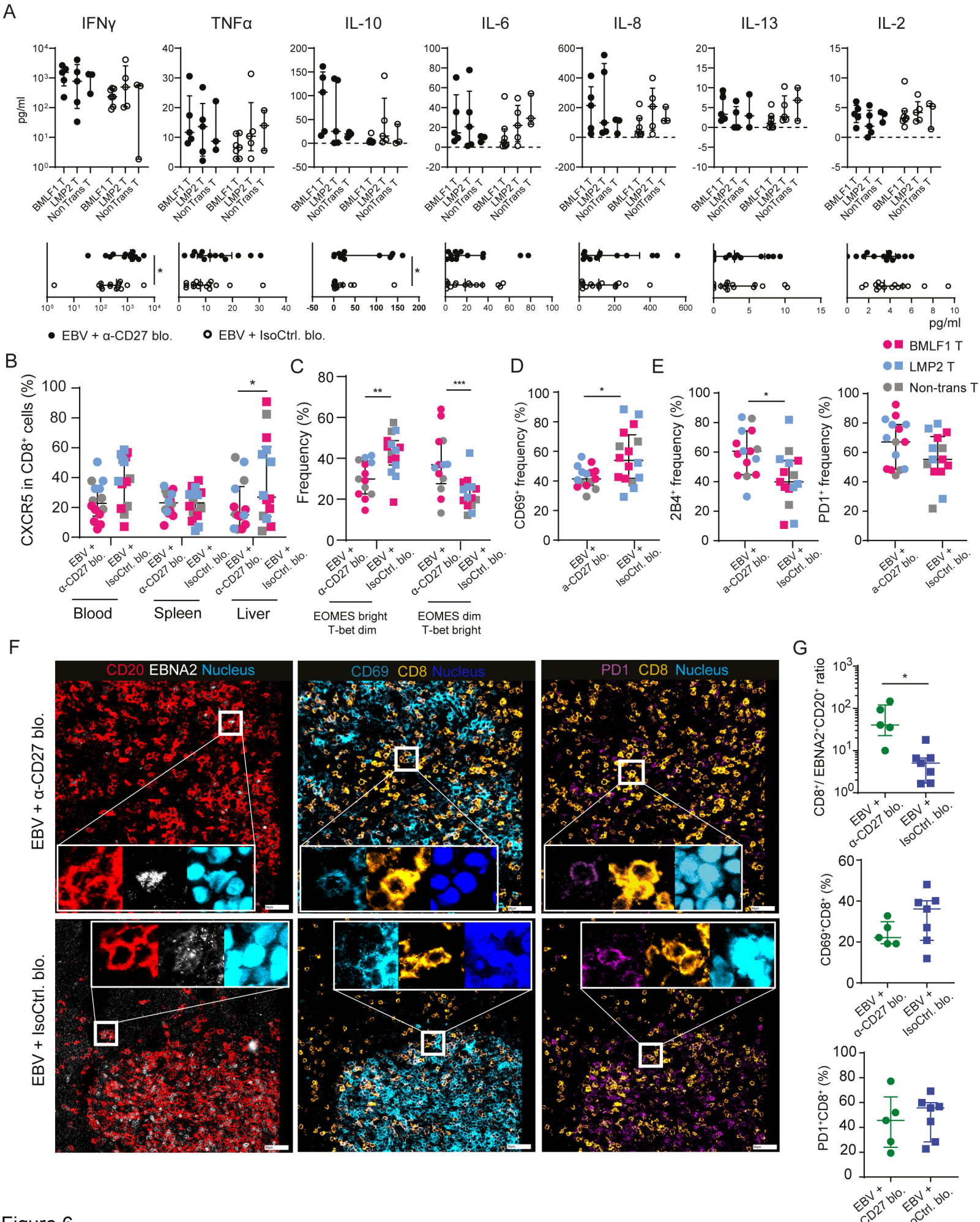
A
IFNγ
TNFα
IL-10
IL-6
IL-8
IL-13
IL-2
pg/ml
BMLF1 T
LMP2 T
NonTrans T
EBV + α-CD27 blo.
EBV + IsoCtrl. blo.
B
CXCR5 in CD8⁺ cells (%)
Blood
Spleen
Liver
C
Frequency (%)
EOMES bright T-bet dim
EOMES dim T-bet bright
D
CD69⁺ frequency (%)
E
2B4⁺ frequency (%)
PD1⁺ frequency (%)
BMLF1 T
LMP2 T
Non-trans T
F
CD20 EBNA2 Nucleus
CD69 CD8 Nucleus
PD1 CD8 Nucleus
EBV + α-CD27 blo.
EBV + IsoCtrl. blo.
G
CD8⁺/ EBNA2⁺CD20⁺ ratio
CD69⁺CD8⁺ (%)
PD1⁺CD8⁺ (%)

Figure 6

# CD27 is required for protective lytic EBV antigen specific CD8$^+$ T cell expansion

Yun Deng, Bithi Chatterjee, Kyra Zens, Hana Zdimerova, Anne Müller, Patrick Schumachers, Laure-Anne Ligeon, Antonino Bongiovanni, Riccarda Capaul, Andrea Zbinden, Angelika Holler, Hans Stauss, Wolfgang Hammerschmidt and Christian Münz

## Supplementary Figure Legends

**Figure S1. Related to Figure 1. Gating strategy of CD27$^+$ cells in huMice**

(A) Representative flow cytometry gating strategy of CD27$^+$ cells in different immune cell populations in huMice.

**Figure S2. Related to Figure 2. CD27 depletion effect on T and B cells**

(A) Flow cytometry analysis of CD3$^+$ T cells -1 (before), 1 and 6 days post injection of anti-CD27 depletion antibody.

(B) Total numbers of CD19$^+$ B cells at the end of experiment as compared between anti-CD27 depletion antibody-treated group (n= 9-13 per group) and isotype control antibody-treated group (n= 8-11 per group). Mann-Whitney test was used to analyze the p value; ns: not significant. Data are pooled from two independent experiments.

**Figure S3. Related to Figure 3. CD27 blocking antibody does not deplete CD27$^+$ cells, and no significant difference in EBV viral loads between groups with transferred BMLF1 and LMP2 specific T cells could be observed.**

(A-B) Frequency of CD3$^+$ T cells (A) and CD19$^+$ B cells (B) in the respective group (left) and total cell count (right) in peripheral blood and spleen at termination of experiment.

(C) Graphical illustration describing the working principle of using two fluorochrome-conjugated anti-CD27 antibodies to check the blocking effect of the blocking antibody.

(D) Frequency of CD27$^+$ CD8$^+$ T cells detected by anti-CD27 antibody derived from a different clone to the injected anti-CD27 blocking antibody.

(E) Frequency of CD27$^+$ CD8$^+$ T cells detected by anti-CD27 antibody derived from the same clone as the injected anti-CD27 blocking antibody.

(F) Longitudinal data of animal weight over time until termination in the respective groups.

(G) Animal survival over time until experiment termination in the respective groups.
(H) Comparison of EBV viral loads in different transfer conditions in blood (left), spleen (middle) and liver (right).
(I) Frequency of CD27 positive of $EBNA2^+$ B cells in blood (left) and spleen (right).
(J) qRT-PCR analysis shows relative gene expression of the representative five EBV latent genes and five lytic genes in the anti-CD27 blocking antibody-treated group versus isotype control antibody treated group. Data are normalized to housekeeping gene SDHA expression. n= 4 from one out of three independent experiments.
(K-L) Representative immunohistochemistry images of EBNA2 in the respective groups, original magnification 200x (K), and the quantification of $EBNA2^+$ cells/$mm^2$ in splenic sections (L).
Data (n= 14-16 per group) are pooled from two independent mouse experiments in graph (A) and (C-H) and displayed with median and interquartile range. Two-way ANOVA analysis and Sidak's multiple comparisons as a post hoc test was used for (C -F) and (I), Mann-Whitney test for (A), two-way ANOVA analysis and Tukey's multiple comparisons for (H) to assess p values. Log-rank (Mantel-Cox) test for (G) was used to compare the survival curves. One-way ANOVA analysis (Kruskal-Wallis test) followed by Tukey's post hoc test was used for (L). Graph I (n=4-6 per group) is from one experiment and Mann-Whitney test was used to assess the p values: *$p<0.05$, **$p<0.01$, ***$p<0.001$. ns: not significant.

**Figure S4. Related to Figure 4. Individual expression and co-expression of CD39, CD70, Ki67 and EBNA2 in blood and spleen under CD27 blockade**

(A-B) UMAP presentation overlaid expression of each individual marker in blood (A) and spleen (B).
(C) Representative UMAP analysis depicts clusters, showing the co-expression of CD39, CD70, Ki67 and EBNA2 on the $CD19^+$ B cells in spleen.
(D) Transformed data from (C) are shown in frequency of each population in different experimental groups.
(E) Representative heatmap analysis of co-expression of CD39, CD70, Ki67 and EBNA2 on $CD19^+$ B cells in spleen.

Graphs (A-E) (n= 7-8 per group) are representative from one out of two independent experiments.

**Figure S5. Related to Figure 5. Treatment with anti-CD27 blocking antibody shows no effect on T cell memory subsets *in vivo* and LCL proliferation *ex vivo***

(A) Comparison of T cell memory subsets characterized by CD45RA and CD62L expression and depicted as naïve, Tcm, Tem and Temra cells in different transfer conditions (BMLF1 and LMP2) in blood (from one representative experiment).

(B) T cell memory subsets in groups treated with either anti-CD27 blocking antibody or isotype control antibody *in vivo*. Cells were harvested at termination of experiment from spleen, liver and bone marrow.

(C) Flow cytometry plots of LCL proliferation. Three LCLs generated from human cells and huNSG/huNSG-A2 mice, respectively, were labeled with Cell Trace Violet and incubated with either anti-CD27 blocking antibody (10μg/mL) or isotype control antibody (10μg/mL) for 3 and 10 days.

Data (n=3 per group) in graph A is from one representative experiment. Data (n= 5-6 per group) in graph B are pooled from two independent experiments and displayed with median and interquartile range. Mann-Whitney test was used to assess p values; *$p<0.05$, **$p<0.01$.

**Figure S6. Related to Figure 6.**

(A) Overview of the CD20, CD8 and EBNA2 stainings in whole spleen sections after anti-CD27 blocking or isotype control antibody treatment, acquired by ChipCytometry. Big bright red and green spots in the isotype treatment condition are artifacts during acquisition.

(B) Frequency of $CD8^+$ T cells and $EBNA2^+CD20^+$ B cells as quantified in 5 to 7 randomly chosen positions.

(C) Immunofluorescence images for human CD45, CD7, CD38, the linage markers CD3, CD4, CD8, CD21 and CD11c.

(D) Immunofluorescence images for CD45RA, CD45RO and CD62L used to define T cell subsets.

(E) Immunofluorescence images for co-stimulatory/inhibitory molecules CD27, CD28, CD30, TIM3, CD278, CD40, CD134 (OX40 receptor) and the transcription factor FoxP3.

(F) Immunofluorescence images for CD39, HLADR, and Ki67.

Scale bars for (A), (C)-(F) are 50μm.

A

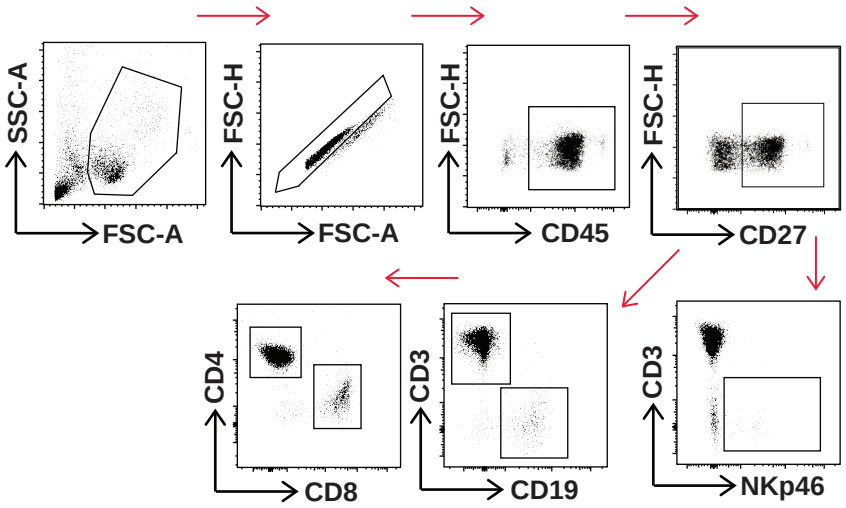
SSC-A
FSC-A
FSC-H
FSC-A
FSC-H
CD45
FSC-H
CD27
CD4
CD8
CD3
CD19
CD3
NKp46

Figure S1

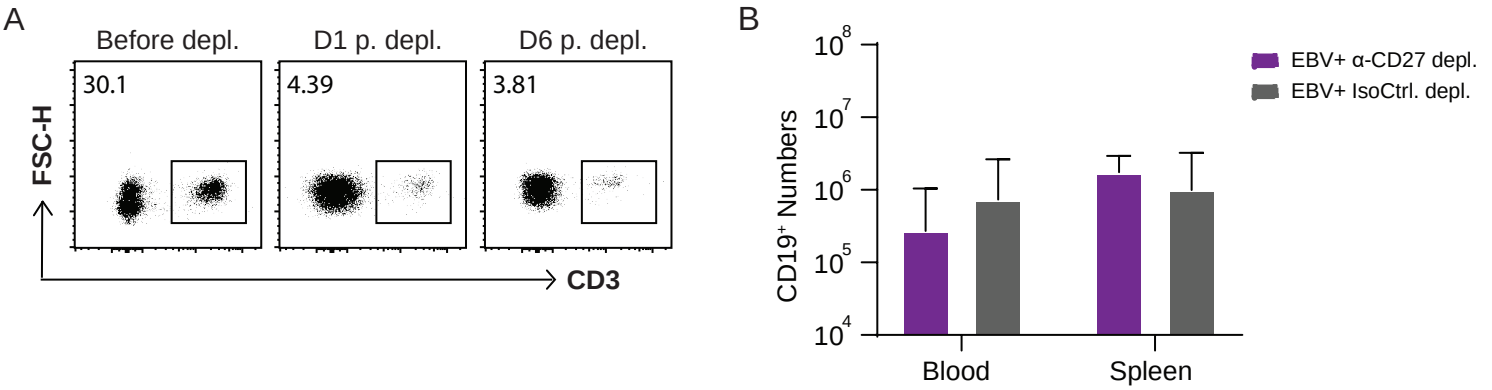
A
Before depl.
D1 p. depl.
D6 p. depl.
30.1
4.39
3.81
FSC-H
CD3
B
EBV+ α-CD27 depl.
EBV+ IsoCtrl. depl.
CD19+ Numbers
10^8
10^7
10^6
10^5
10^4
Blood
Spleen

Figure S2

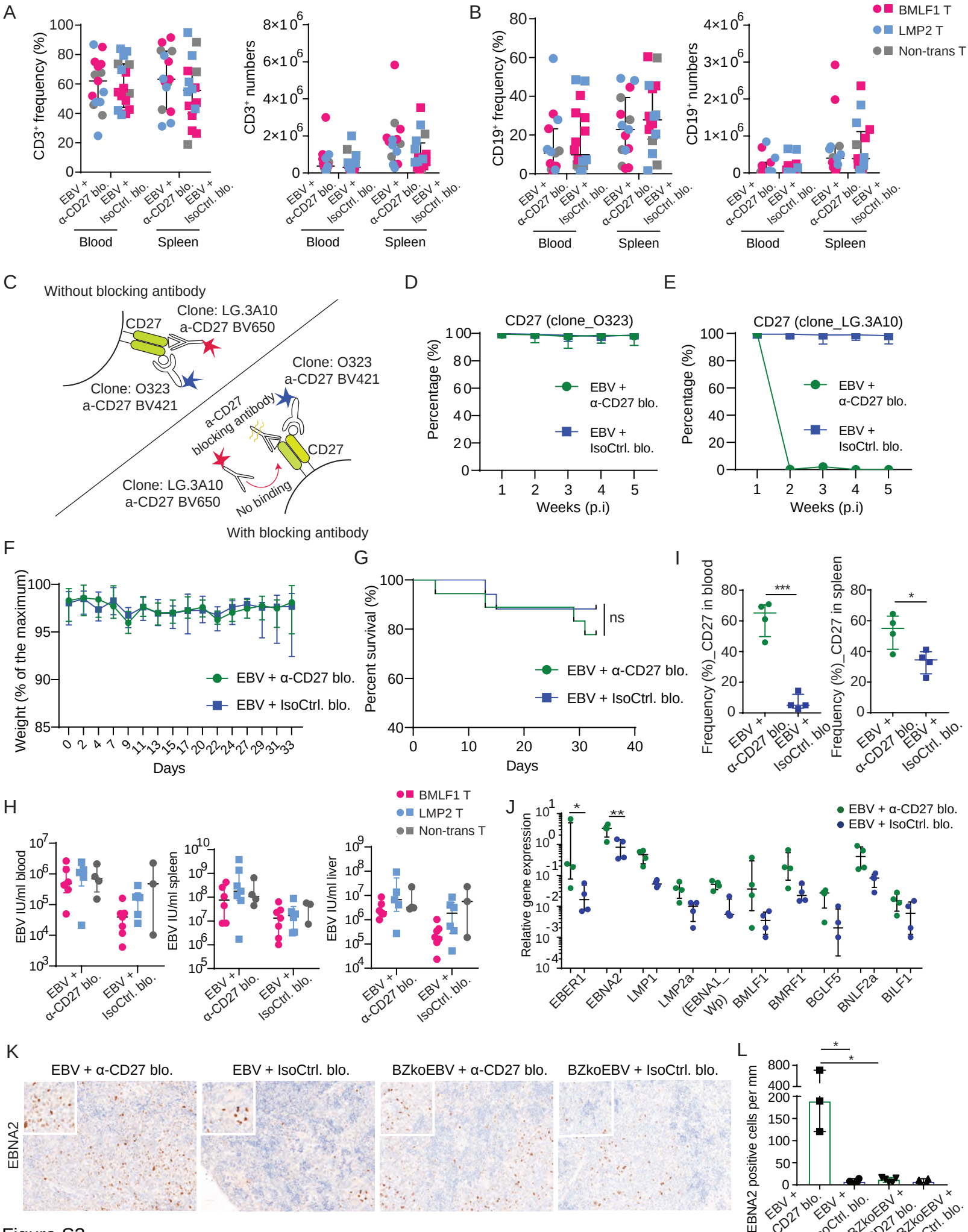
A
CD3+ frequency (%)
CD3+ numbers
EBV + α-CD27 blo.
EBV + IsoCtrl. blo.
Blood
Spleen
B
CD19+ frequency (%)
CD19+ numbers
BMLF1 T
LMP2 T
Non-trans T
C
Without blocking antibody
CD27
Clone: LG.3A10
a-CD27 BV650
Clone: O323
a-CD27 BV421
With blocking antibody
a-CD27 blocking antibody
No binding
D
CD27 (clone_O323)
Percentage (%)
Weeks (p.i)
E
CD27 (clone_LG.3A10)
F
Weight (% of the maximum)
Days
G
Percent survival (%)
ns
I
Frequency (%)_CD27 in blood
Frequency (%)_CD27 in spleen
H
EBV IU/ml blood
EBV IU/ml spleen
EBV IU/ml liver
J
Relative gene expression
EBER1
EBNA2
LMP1
LMP2a
(EBNA1_ Wp)
BMLF1
BMRF1
BGLF5
BNLF2a
BILF1
K
EBV + α-CD27 blo.
EBV + IsoCtrl. blo.
BZkoEBV + α-CD27 blo.
BZkoEBV + IsoCtrl. blo.
EBNA2
L
EBNA2 positive cells per mm

Figure S3

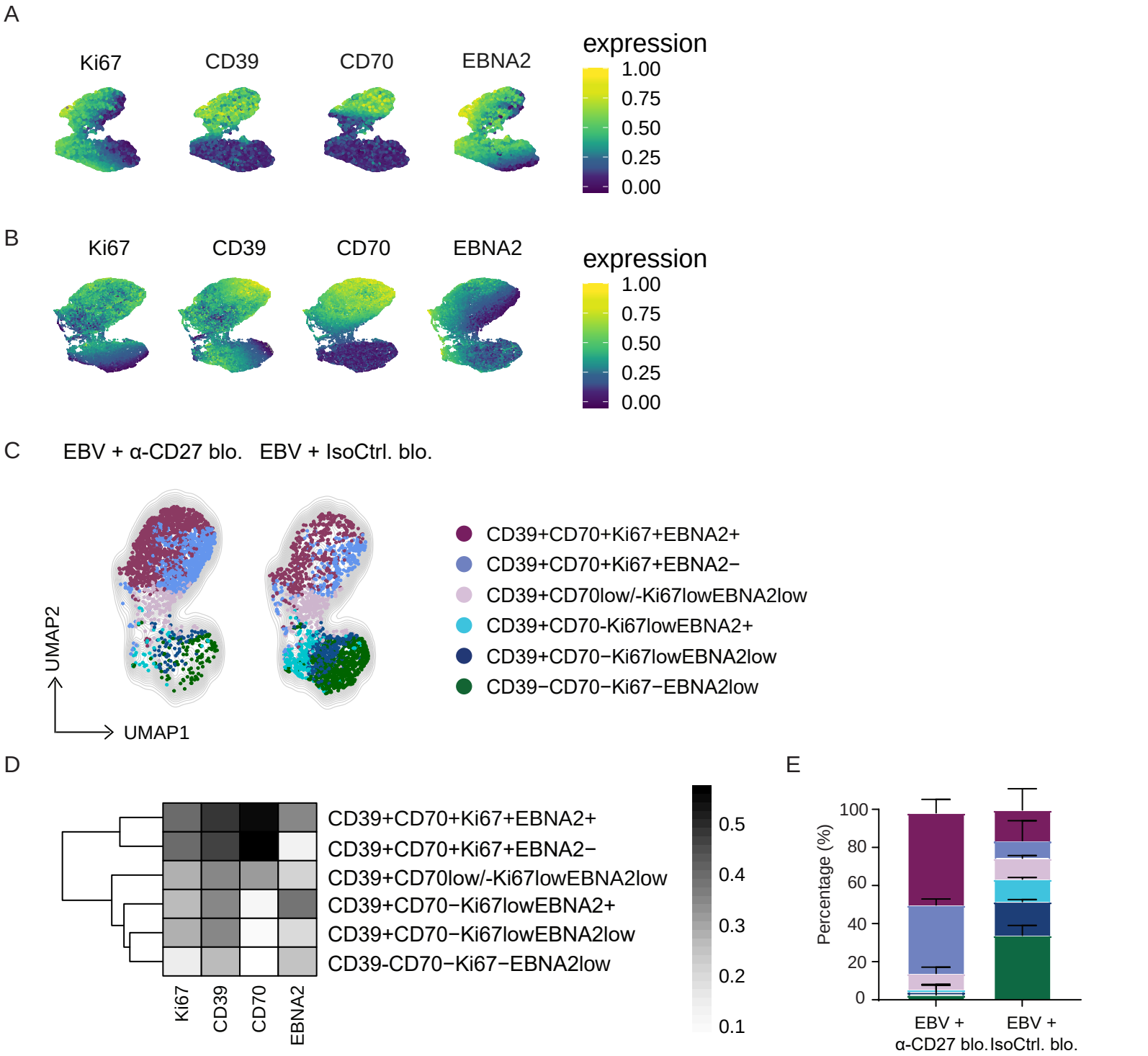
A
Ki67
CD39
CD70
EBNA2
expression
1.00
0.75
0.50
0.25
0.00
B
Ki67
CD39
CD70
EBNA2
expression
1.00
0.75
0.50
0.25
0.00
C
EBV + α-CD27 blo.
EBV + IsoCtrl. blo.
UMAP2
UMAP1
CD39+CD70+Ki67+EBNA2+
CD39+CD70+Ki67+EBNA2−
CD39+CD70low/-Ki67lowEBNA2low
CD39+CD70-Ki67lowEBNA2+
CD39+CD70−Ki67lowEBNA2low
CD39−CD70−Ki67−EBNA2low
D
CD39+CD70+Ki67+EBNA2+
CD39+CD70+Ki67+EBNA2−
CD39+CD70low/-Ki67lowEBNA2low
CD39+CD70−Ki67lowEBNA2+
CD39+CD70−Ki67lowEBNA2low
CD39-CD70−Ki67−EBNA2low
Ki67
CD39
CD70
EBNA2
0.5
0.4
0.3
0.2
0.1
E
Percentage (%)
100
80
60
40
20
0
EBV + α-CD27 blo.
EBV + IsoCtrl. blo.

Figure S4

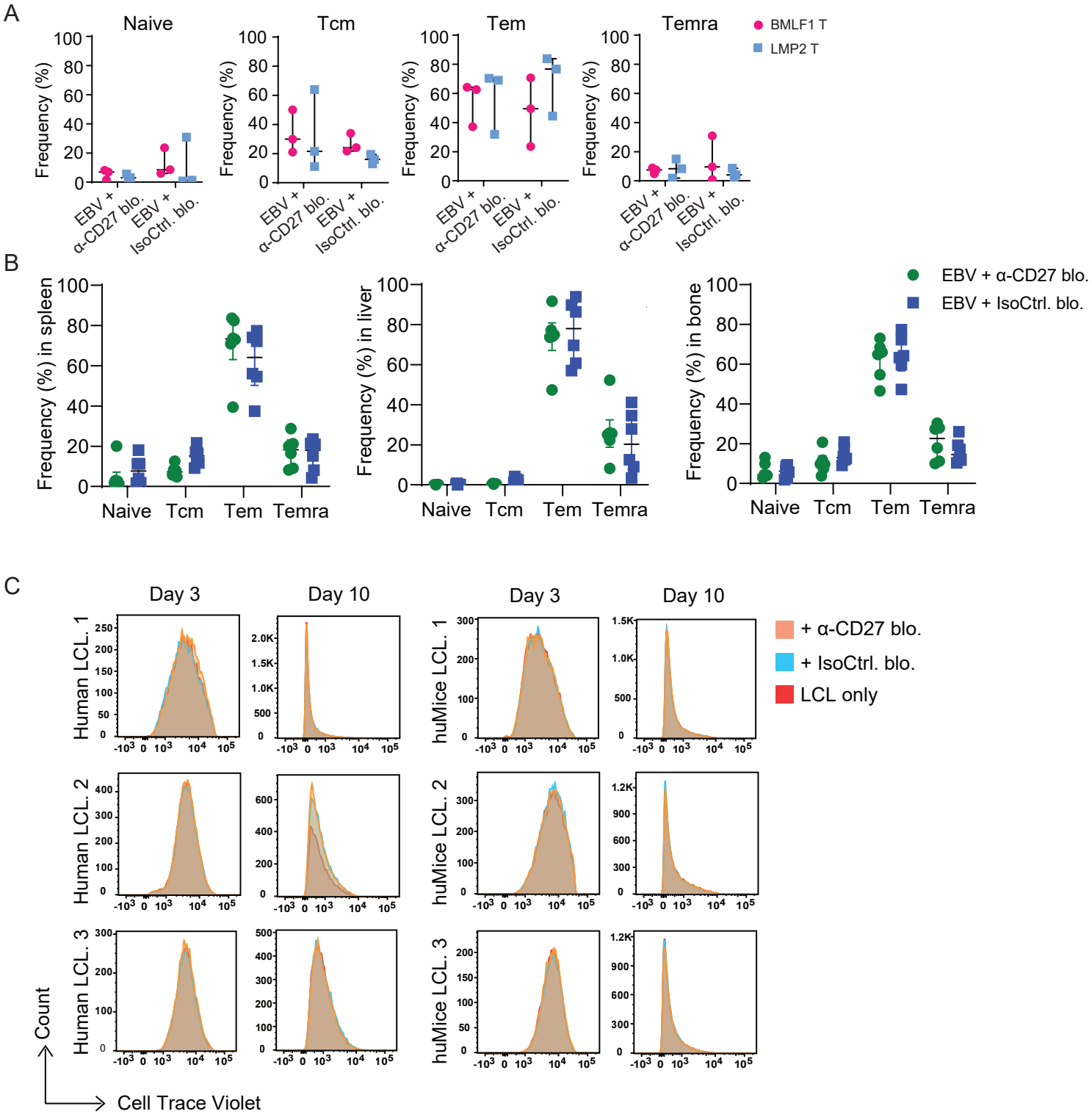
A
Naive
Tcm
Tem
Temra
BMLF1 T
LMP2 T
Frequency (%)
EBV + α-CD27 blo.
EBV + IsoCtrl. blo.
B
Frequency (%) in spleen
Frequency (%) in liver
Frequency (%) in bone
EBV + α-CD27 blo.
EBV + IsoCtrl. blo.
Naive
Tcm
Tem
Temra
C
Day 3
Day 10
Human LCL. 1
Human LCL. 2
Human LCL. 3
huMice LCL. 1
huMice LCL. 2
huMice LCL. 3
+ α-CD27 blo.
+ IsoCtrl. blo.
LCL only
Count
Cell Trace Violet

Figure S5

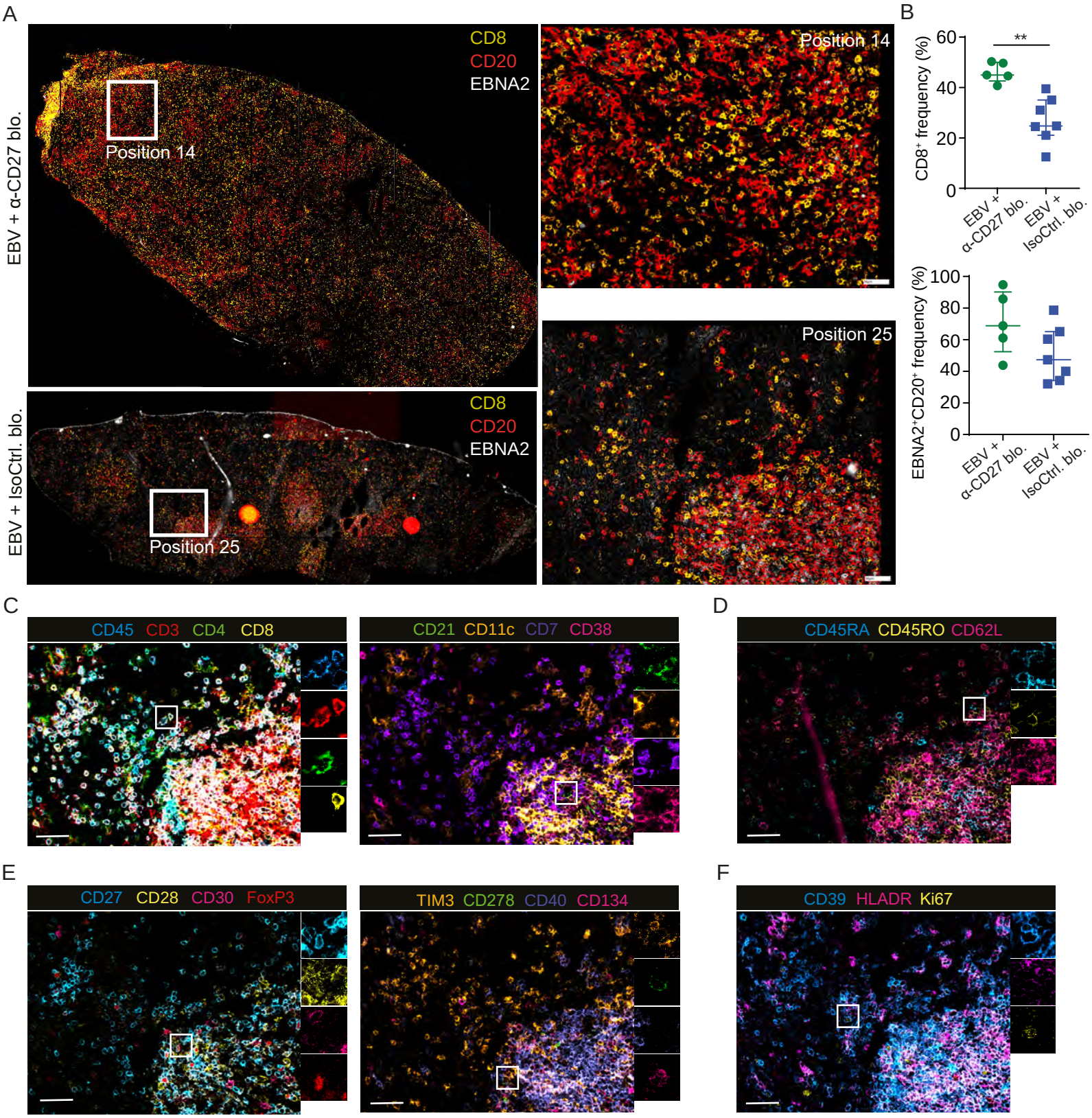
A
EBV + α-CD27 blo.
CD8
CD20
EBNA2
Position 14
Position 14
EBV + IsoCtrl. blo.
CD8
CD20
EBNA2
Position 25
Position 25
B
CD8+ frequency (%)
60
40
20
0
**
EBV + α-CD27 blo.
EBV + IsoCtrl. blo.
EBNA2+CD20+ frequency (%)
100
80
60
40
20
0
EBV + α-CD27 blo.
EBV + IsoCtrl. blo.
C
CD45 CD3 CD4 CD8
CD21 CD11c CD7 CD38
D
CD45RA CD45RO CD62L
E
CD27 CD28 CD30 FoxP3
TIM3 CD278 CD40 CD134
F
CD39 HLADR Ki67

Figure S6

Table S1: Antibodies and dyes for ChipCytometry

| | Markers | Color | Clone | Company | Cat# |
|---|---|---|---|---|---|
| 1 | CD8 | PerCP | SK1 | Biolegend | 344708 |
| 2 | CD4 | PE | RPA-T4 | Biolegend | 300508 |
| 3 | CD45 | BUV395 | HI30 | BD | 563792 |
| 4 | CD45RA | FITC | HI100 | BD | 555488 |
| 5 | CD11c | PE | S-HCl-3 | Biolegend | 371504 |
| 6 | CD27 | PerCP | LG.3A10 | Biolegend | 124213 |
| 7 | CD134 (OX40) | PE | Ber-Act35 | Biolegend | 350003 |
| 8 | CD278 (ICOS) | PerCP | C398.4A | Biolegend | 313517 |
| 9 | CD45RO | FITC | UCHL1 | BD | 555492 |
| 10 | CD3 | PE | SK7 | Biolegend | 344805 |
| 11 | CD56 | PE | MEM-188 | BL | 304605 |
| 12 | CD69 | PE | FN50 | Biolegend | 310905 |
| 13 | CD38 | PE | HIT2 | Biolegend | 303506 |
| 14 | CD30 | PE | Ber-H8 | BD | 550041 |
| 15 | CD20 | PE | 1412 | Biolegend | 340510 |
| 16 | CD40 | FITC | HB14 | Biolegend | 313004 |
| 17 | CD7 | FITC | CD7-6B7 | Biolegend | 343104 |
| 18 | CD62L | PE | FMC46 | BioRad | MCA1076PET |
| 19 | CD279 (PD1) | PE | EH12.1 | BD | 560795 |
| 20 | HLA-DR | FITC | G46.6 | BD | 555811 |
| 21 | CD28 | PE | CD28.2 | BD | 5585729 |
| 22 | CD21 | PE | Bu32 | Biolegend | 354921 |
| 23 | CD366 (TIM3) | PE | D5D5R | RD | FAB2365P |
| 24 | Ki67 | PE | B56 | BD | BD 556027 |
| 25 | FOXP3 | PE | 236A/E7 | BD | 560852 |
| 26 | CD39 | FITC | A1 | Biolegend | 328207 |
| 27 | EBNA2 | PE | R3 | Sigma | MABE8 |
| 28 | Helix NP Green | FITC | | Biolegend | 425303 |

Table S2. Quantitative RT-PCR primer list in the paper.

| Name | Primer/Probe | Source | Sequence |
|---|---|---|---|
| EBER1 | F | Tierney et al., 2015 | TGCTAGGGAGGAGACGTGTGT |
| | R | | TGACCGAAGACGGCAGAAAG |
| | probe | | AGACAACCACAGACACCGTCCTCACCA |
| EBNA2 | F | Bell et al., 2006 | GCTTAGCCAGTAACCCAGCACT |
| | R | | TGCTTAGAAGGTTGTTGGCATG |
| | probe | | CCCAACCACAGGTTCAGGCAAAACTTT |
| LMP1 | F | Bell et al., 2006 | AATTTGCACGGACAGGCATT |
| | R | | AAGGCCAAAAGCTGCCAGAT |
| | pobe | | TCCAGATACCTAAGACAAGTAAGCACCCGAAGAT |
| LMP2a | F | Bell et al., 2006 | CGGGATGACTCATCTCAACACATA |
| | R | | GGCGGTCACAACGGTACTAACT |
| | probe | | CAGTATGCCTGCCTGTAATTGTTGCGC |
| EBNA1 (Wp) | F | Bell et al., 2006 | TGCCTGAACCTGTGGTTGG |
| | R | | CATGATTCACACTTAAAGGAGACGG |
| | probe | | TCCTCTGGAGCCTGACCTGTGATCG |
| BMLF1 | F | Tierney et al., 2015 | CCCGAACTAGCAGCATTTCCT |
| | R | | GACCGCTTCGAGTTCCAGAA |
| | probe | | AACGAGGATCCCGCAGAGAGCCA |
| BMRF1 | F | Tierney et al., 2015 | GAGGAACGAGCAGATGATTGG |
| | R | | TGCCCACTTCTGCAACGA |
| | probe | | TGCTGTTGATGCCCAAGACGGCTT |
| BGLF5 | F | Tierney et al., 2015 | GCAAGCCCGGGAGAGACT |
| | R | | GAGGCGACCGTTTTCGAA |
| | probe | | CGGGTGAACATTGTGACGGCCTTC |
| BNLF2a | F | Tierney et al., 2015 | TGGAGCGTGCTTTGCTAGAG |
| | R | | GGCCTGGTCTCCGTAGAAGAG |
| | probe | | CCTCTGCCTGCGGCCTGCC |
| BILF1 | F | Tierney et al., 2015 | TGCCTTTTGACCCAGAACATG |
| | R | | CAACGCCATACCCAAGTGAGT |
| | probe | | TACGGAGCACATCAGGCCCAAGAACA |

## Supplementary Methods

### Humanized mouse generation and infection

NOD-scid $\gamma_c^{null}$ (NSG) mice and HLA-A2 transgenic NSG mice were originally purchased from Jackson Laboratories (Bar Harbor, Maine, USA) and maintained in ventilated, specific pathogen-free cages at the Institute of Experimental Immunology, University of Zurich. To assist with the engraftment of human $CD34^+$ hematopoietic progenitor cells (HPCs), newborn pups (1-5 days) were irradiated with 1Gy prior to reconstitution [1,2]. Five to seven hours later, irradiated pups were intrahepatically injected with $2x10^5$ $CD34^+$ human hematopoietic progenitor cells (HPCs) isolated from human fetal livers (HFL) (Advanced Bioscience Resources, USA). The HFL samples were procured during termination between gestational weeks 14 and 22. Use of human tissue was approved by the cantonal ethics committee of Zurich (KEK-ZH-Nr. 2010-0057 and 2019-00837). After 12 weeks of reconstitution, peripheral blood was collected via tail vein bleeding and cells were checked for immune cell populations through expression of human CD45, CD3, CD4, CD8, CD19, NKp46 and HLA-DR, as previously described [3]. All procedures were strictly followed in accordance with the animal protocols ZH209/2014 & ZH159/17, licensed by the veterinary office of the canton of Zurich, Switzerland. Mice were immune phenotyped again prior to the start of the experiments and showed the following mean frequencies of different cell populations; $huCD45^+$ 81.5% ± 8.5%, $huCD3^+$ T cells of $huCD45^+$ 33.6% ± 10.9%, $huCD19^+$ B cells of $huCD45^+$ 53.9% ± 12.1%, $huCD4^+$ T cells of human T cells 74.5% ± 8.6%, $huCD8^+$ T cells of human T cells 22.4% ± 8.2% and $NKp46^+$ NK cells of $huCD45^+$ 3.2% ± 1.9%. Animals were used between 12 and 28 weeks old (Mean ± SD, n = 80; female 43 and male 37). Mice were then injected with $10^5$ Raji Green units (RGU) of wild type Epstein Barr virus (EBV) or Luciferase-expressing EBV (Luc-EBV) intraperitoneally (i.p.) and monitored for 4 to 6 weeks. In each experimental group, 3 to 6 biological replicates were tested. For each individual experiment, animals were reconstituted from a single HFL donor and distributed into different experimental groups with a similar ratio of males and females, as well as similar reconstitution levels of human immune cell populations.

### Wild type EBV, BZLF1 knock-out EBV and Luciferase-expressing EBV production

Wild type EBV B95-8 strain-producing cells were a generous gift of Prof. Dr. Henri-

Jacques Delecluse (DKFZ, Heidelberg, Germany). The recombinant EBV B95-8 DNA was stored as a bacmid and encompassed the gene for hygromycin resistance and green fluorescent protein (GFP) in HEK293 cells. Similarly, EBV B95-8-delta BZLF1 knock-out EBV (BZkoEBV) was produced in HEK293 cells. Those cells were cultured in DMEM (1X) medium supplemented with 10% heat inactivated FBS, 20µg/ml gentamycin and 20µg/ml hygromycin. Cell transfection was performed using 3 µg of BZLF1 (p509) and BALF4 (p2670) plasmids each, together with 32 µl of METAFECTENE® PRO (Biontex) in 10 cm petri dishes [3-5]. The virus supernatant was harvested 3 days after transfection and concentrated through centrifugation at 30,000g for 2 hours at 4 °C. Prior to animal infection, the GFP expressing virus was titrated on Raji cells *in vitro* by analyzing the GFP positive cells 48h after infection with flow cytometry. Based on the serial dilution of the virus on Raji cells, Raji Green units (RGU) were calculated for each virus preparation. Luciferase-expressing EBV (Luc-EBV) producer cells were kindly provided by Prof. Dr. Wolfgang Hammerschmidt (HelmholtzZentrum, Munich, Germany). Luc-EBV genome was originally derived from the B95-8 EBV with bioluminescent firefly luciferase protein incorporated as an EBV EBNA2 fusion construct and produced in HEK293 cells. It was produced and titrated in the same way as described above for wild type and BZLF1 knock-out EBV, if not stated otherwise.

**EBV-specific T cell receptor (TCR) generation and adoptive T cell transfer**

Phoenix-AMPHO packaging cells were transfected with envelope vector pCl-Ampho construct and either LMP2-TCR or BMLF1-TCR to produce retrovirus supernatants encoding EBV-specific TCRs. Subsequently, CD3/CD28 Dynabeads (Thermofisher Scientific) activated splenocytes derived from donor-mate animals were transduced with either LMP2-TCR or BMLF1-TCR encoding retroviruses. Transduction efficiency was determined by flow cytometry 48 hours after the second transduction. A total of 200'000 $TCR^{+}CD3^{+}$ T cells were transferred intravenously into donor-matched recipient mice and monitored longitudinally during the course of EBV infection.

***In vivo* bioluminescence imaging**

The progression of EBV infection was monitored longitudinally every week and quantitatively measured by *in vivo* bioluminescence imaging with the IVIS Spectrum

Imaging System (PerkinElmer). Animals were anesthetized by isofluorane with the flow of 3 liters per minute and injected i.p. with 150mg/kg D-Luciferin (Promega) 10 minutes before imaging. Mice were placed inside the IVIS imaging box and imaged dorsally and ventrally. Representative images were acquired at 2 minutes for each mouse during the entire experiment to illustrate the virus progression within the host. Images for quantification were captured at various time points before the luminescent signal reached the saturation intensity and analyzed with Living image 4.3.1 software (PerkinElmer). Regions of interest (ROI) were set to include the regions with luminescent signal in mice and photon flux (p/s) of light emitted per second within the ROI was measured as the readout.

**Preparation of tissue sections for ChipCytometry**

Splenic tissues from EBV infected mice treated with either anti-CD27 blocking antibody or the corresponding isotype control antibody were collected at the termination of experiment. Vertically dissected fresh tissues, up to 0.5cm in thickness were embedded in OCT (Tissue-Tek) and preserved at -80°C. Tissue sectioning was prepared on a cryostat (Leica) instrument by placing the frozen tissue block facing up on a freezing-temperature steel well and adjusting the temperature of the chamber and cutting knife to -16°C and -17°C, respectively. The section thickness was set to 5-6µm. Each individual section was collected on a room temperature microscope cover slide and assembled into a ZellSafe_T chip (Canopy Biosciences). Tissue on the cover slide was fixed using 100% acetone for 5 minutes, 90% ethanol for 3 minutes, 70% ethanol for 3 minutes on ice and washed twice with PBS.

**Antibody staining and tissue immunofluorescence imaging in ChipCytometry**

Prior to staining of the samples, individual antibodies were filtered and titrated to their optimal dilution to achieve a good signal-to-background staining, known as the optimal Fisher's discrimination ratio (FDR). Tissues on the chips were blocked using blocking buffer (1% fetal bovine serum, 10% normal mouse serum and 0.1% Tween-20 in PBS) for one hour at room temperature. For surface staining, the relevant monoclonal antibodies were prepared in 400µl of blocking buffer and incubated with the sample for 15 minutes at either four degrees or at room temperature, depending on the optimized staining condition per antibody. Followed by a continuous wash step with PBS containing 0.1% Tween-20 controlled by an automated Ismatec pump

system for 5 minutes and washing the chip twice with PBS, the chip was ready to be acquired. For the intranuclear staining, tissue was permeabilized using 1X perm buffer from the FoxP3 Transcription factor staining buffer set (Invitrogen), washed with PBS and incubated with antibodies for intranuclear markers for 15 minutes before washing. For the EBNA2 staining, tissue was blocked with blocking buffer containing 10% normal mouse serum, 1% FCS, 0.1% Tween 20 in 1X perm buffer for 1 hour. Purified primary EBNA2 rat anti-human antibody was applied in blocking buffer for 1 hour at 4°C. Followed by washing with 0.1% Tween 20, tissue was incubated with secondary mouse anti-rat IgG2a PE antibody (Biolegend) in blocking buffer for 15 minutes at room temperature, and then washed with PBS-0.1% Tween 20 before acquisition.

Combining Zellkraftwerk ZellScanner One and ZellExplorer software, fluorescent antibody-labeled tissue samples were acquired. Briefly, each chip was photobleached in all channels and scanned for background fluorescence. A whole slide scan was ordered in the beginning in order to have full spatial information about the tissue. After staining with the corresponding antibodies, the fluorescent signals were acquired and then photobleached preparing for the next round of acquisition of background fluorescence and fluorescent signals of antigens of interest. In the end, the net fluorescent signal was achieved and calculated by deducting the background fluorescence in each staining round. 28 parameters were assessed in the splenic tissue sections (Table S1).

**Quantification of EBV DNA genome in blood and tissue**

Total DNA from whole blood and small pieces of spleen and liver was extracted using NucliSENS easyMag (Biomerieux) and DNeasy Blood & Tissue Kit (QIAGEN) respectively, according to manufacturer's instructions. TaqMan (Applied Biosystems) real-time PCR was used to quantify EBV DNA as previously described [6], with modified primers for the BamH1 W fragment (50-CTTCTCAGTCCAGCGCGTTT-30 and 50-CAGTGGTCCCCCTCCCTAGA-30) and a fluorogenic probe (50-FAM CGTAAGCCAGACAGCAGCCAATTGTCAG-TAMRA-30). All samples were performed in duplicates and measured on either ViiA$^{TM}$ 7 Real-Time PCR System (ThermoFisher Scientific) or ABI Prism 7300 Sequence Detector (Applied Biosystems) at the Institute of Medical Virology, University of Zurich. Samples below the lower limit of quantification (LLOQ) of 122

International Units (IU)/ml were defined as negative for EBV DNA. EBV-inoculated animals with blood and splenic EBV DNA genome below the LLOQ were considered non-infected and excluded from further analysis.

**Cell isolation and tissue preparation**

Peripheral blood cells were obtained from the animals by tail vein bleeding and lysed with 1xACK lysis buffer for 5 minutes, followed by washing with PBS. Splenocytes were prepared as described above. Liver tissues were mechanically chopped into small pieces and enzymatically digested in 2ml of digestion buffer (1mg Collagenase D (Roche) and 0.2mg DNase I (Roche) in 2ml DMEM) at 37°C for 30 minutes with agitation. Dissociated livers were then passed through a 70μm cell strainer and subjected to centrifugation in a discontinuous Percoll gradient (40% and 70%, Sigma-Aldrich) for 20 minutes at 1000rpm. Cells aggregated at the interface between 40% and 70% Percoll gradient were harvested and washed twice with PBS. Bone marrow cells were flushed out of the femur by short centrifugation. Cells were washed with PBS and passed through a 70μm cell strainer if necessary. Cells from different organs were counted using the Beckman Coulter AcT diff Analyzer to aliquot the optimal number of cells for staining and calculation of the total cell numbers for different experimental purposes.

**Antibody, pentamer labeling and flow cytometry**

Surface staining was performed by incubating cells with the relevant mAbs for 20 minutes at 4°C, followed by washing with PBS twice and resuspending in fixation buffer (1% paraformaldehyde) before acquisition. For intracellular staining, cells were labeled with mAbs against surface markers and fixed in fixation buffer as stated above. Then, cells were permeabilized by two washes with PBS+0.05% saponin (PS), resuspended with mAbs against intracellular markers diluted in PS and incubated for 20 minutes at 4°C. For intranuclear staining, cells labeled with mAbs against surface markers were fixed and permeabilized with Foxp3/Transcription Factor Staining Buffer Set (eBioscience) and stained with mAbs against intranuclear markers for 1 hour at 4°C. To detect EBV specific $CD8^+$ T cells, PE-conjugated pentamers specific for BMLF1 and LMP2 antigens, restricted by HLA-$A^*$0201 (Proimmune), were incubated with the cells prior to surface staining for 10 minutes at room temperature [2]. Labeled cells were acquired on either the BD FACSCantoII, BD LSRFortessa or BD

FACSymphony. The data analysis was performed using FlowJo software (FlowJo LLC).

**In vitro-transformed LCL generation**

To generate NSG LCLs *ex vivo*, $CD19^+$ B cells were isolated from the spleen using positive selection with CD19 microbeads according to the manufacturer's recommendations (Miltenyi Biotec). A total of $5x10^5$ cells/well were plated in a 96-well U-bottom plate and cultured with EBV supernatants with a MOI of 0.5. Cells were cultured in RPMI 1640 medium supplemented with 10% heat inactivated FBS, 50U/ml penicillin-streptomycin and 1% L-glutamine. Cell growth was monitored by light microscopy and clusters of cells were normally visible 2 weeks post EBV infection. Outgrowing cells were further expanded by seeding at $3\text{-}5x10^5$ cells/ml and splitting at a concentration of $10^6$ cells/ml.

**Generation of EBV specific $CD8^+$ T cell clones and T cell re-stimulation**

EBV specific T cell clones for BMLF1 and LMP2 were generated from a healthy HLA-A*0201 positive EBV carrier using BMLF1 and LMP2-specific dextramers, as described previously [3]. Briefly, dextramer positive $CD8^+$ T cells were single-cell sorted and co-cultured with irradiated autologous LCLs and PBMC feeder cells in complete T cell medium supplemented with 1µg/ml PHA and 150U/ml IL-2 [7]. IFNγ secretion was analyzed upon re-stimulation with 1µM of the relevant peptides using enzyme-linked immunosorbent assays (ELISA; MABTECH). Only the T cells, which showed specific responses to the relevant peptide were used for further phenotypic characterization and functional T cell avidity tests in peptide titration assays to confirm the specificity of the respective clones.

For re-stimulation, autologous LCLs were pulsed with either BMLF1 or LMP2 specific peptide (1µM), PBMC feeder cells were stimulated with PHA (5µg/ml) overnight and they were irradiated at 20Gy and 60Gy, respectively. T cell clones specific for BMLF1 and LMP2 were co-cultured with irradiated LCLs and PBMC feeder cells at the ratio of 1:5:50 in complete T cell medium (as stated above) for stimulation and expansion for 1 to 2 weeks before conducting the described experiments.

### *In vitro* cytotoxicity assay

Cytotoxic activity of BMLF1 and LMP2 specific T cell clones against autologous LCLs was evaluated as previously described [1]. In brief, target cells (LCLs) were labeled with PKH-26 (Sigma-Aldrich) for 5 minutes and washed with PBS according to the manufacturer's instructions. T cells, pretreated with either anti-CD27 blocking antibody or the corresponding isotype control antibody for a week at the concentration of 5μg/ml, were co-cultured with the labeled target cells at 10:1, 1:1 and 1:10 effector/target ratios. After 21 hours of incubation, TO-PRO-3-iodide (ThermoFisher Scientific), a membrane-impermeable nuclear counterstain for dead cells, was added to each culture (0.5μM final concentration) and cells were analyzed by flow cytometry. Background and maximum TO-PRO-3-iodide staining was obtained by incubation of target cells with medium and/or heating the cells at 90°C for 15 minutes, respectively. The percentage of specific lysis was calculated with the following formula: ((%TO-PRO-3-iodide$^+$PKH26$^+$ cells in co-culture - %TO-PRO-3-iodide$^+$PKH26$^+$ cells in medium) / (%TO-PRO-3-iodide$^+$PKH26$^+$ cells in max kill - %TO-PRO-3-iodide$^+$PKH26$^+$ cells in medium)) x 100%.

### Histology, immunohistochemistry and immunofluorescence

Tissue sections were excised and fixed in 4% formalin overnight before paraffin embedding (SophistoLab). For immunohistochemistry and immunofluorescence, tissue was prepared in 3μm sections with Leica BOND-MAX or Bond-III automated immunohistochemistry system. Tissue sections were treated with BOND Epitope Retrieval Solution 2 (Leica Biosystem) for antigen retrieval at 100°C for 30 minutes. Stainings were performed with Leica HRP Refine Kit (Leica Biosystem). Briefly, samples were incubated with mAb mouse anti-EBNA2 (Abcam) for 30 minutes, followed by incubation with Post Primary Rabbit anti mouse IgG for 20 minutes and anti-rabbit Poly-HRP-IgG for 15 minutes. 3,3'-Diaminobenzidine tetrahydrochloride (DAB) was the substrate chromogen used to visualize the complex via brown precipitate and hematoxylin counterstaining was performed for the visualization of cell nuclei. All stainings were acquired with a Vectra3 automated quantitative pathology imaging system (PerkinElmer) and analyzed with InForm software to quantify positive staining [8].

### Serum cytokine quantification

Serum samples harvested from cardiac puncture at the termination of experiments were preserved at -20°C until use. Concentration of each individual cytokine (prepared 1:2.5 with dilution buffer) were measured in duplicates using V-PLEX Proinflammatory Panel 1 kits (Mesoscale) following the manufacturer's instructions. Standard dilutions for the calibrator blend for standard curve generation were prepared in parallel in duplicates. Plates were read with a Meso Quickplex SQ120 and analyzed with Discovery Workbench 4.0.12 (Mesoscale) [2,9].

**B cell isolation and quantitative RT-PCR (qRT-PCR)**

Total RNA was isolated with MACS sorting for B cells using CD19 human MicroBeads (Miltenyi Biotec) and extracted using RNeasy Mini Kit (QIAGEN) according to the manufacturer's recommendations. To avoid genomic DNA contamination, the on-column DNase processing was included during the RNA isolation (RNase-Free DNase Set, QIAGEN). cDNA was synthesized in a 20µl volume mixed with reverse transcriptase (Promega) and primer mix at concentrations of 10µM each. qRT-PCR was performed with a CFX384 Touch Real-Time PCR Detection System (Bio-Rad) using a program of 2 minutes at 50°C and 10 minutes at 95°C, followed by 50 cycles of amplification (95°C for 15 seconds and 60°C for 1 minute) [9]. Primers used in this manuscript are listed in Table S2 [10,11]. Transcript level of each gene of interest was calculated relative to the geometric mean of the reference gene *SDHA* (TaqMan Applied Biosystems Gene Expression Assay (Hs00417200)) and presented as relative gene expression.

**Fluorescence image segmentation and quantification**

Quantification of cells positive for EBNA2, CD8, CD20, CD69 and PD1 (single and/or double-positive) was performed using a homemade semiautomatic plugin designed on ImageJ. For every image the channels were separated and cell segmentation were performed on the nuclei channels, then the average of fluorescence intensity for each single protein was measured (the threshold is selected manually for each channel), and followed by quantification. The lineage markers and markers that are expressed on many different types of immune cells are show in Figure S6C; the markers used to characterize the T cell subsets are shown in Figure S6D; the stainings for co-stimulatory molecules and their receptors, as well as FoxP3 that are all positive

for CD27 are shown in Figure S6D; the markers that have high expression on B cells are shown in Figure S6F.

**High-dimensional analysis**

Flow cytometry data was processed using FlowJo software and imported into Cytobank to generate cell density plots and histograms (Beckman Coulter). All the parameters were displayed with an arcsinh transformation with an argument ranging from 50 to 500 on different biomarkers. The exported FCS files, together with the argument information, were uploaded into Rstudio. The FlowSom algorithm was used for automated clustering of cell populations for UMAP and heatmap [12]. Individual cluster frequencies generated in the R environment were exported and used for further analysis.

**References**

1. Strowig T, Gurer C, Ploss A, et al. Priming of protective T cell responses against virus-induced tumors in mice with human immune system components. *J Exp Med*. 2009;206(6):1423-1434.

2. Chatterjee B, Deng Y, Holler A, et al. $CD8^+$ T cells retain protective functions despite sustained inhibitory receptor expression during Epstein-Barr virus infection in vivo. *PLoS Pathog*. 2019;15:e1007748.

3. Antsiferova O, Müller A, Rämer P, et al. Adoptive transfer of EBV specific $CD8^+$ T cell clones can transiently control EBV infection in humanized mice. *PLoS Pathog*. 2014;10(8):e1004333.

4. Chijioke O, Muller A, Feederle R, et al. Human natural killer cells prevent infectious mononucleosis features by targeting lytic Epstein-Barr virus infection. *Cell Rep*. 2013;5(6):1489-1498.

5. Nowag H, Guhl B, Thriene K, et al. Macroautopphagy proteins assist Epstein Barr virus production and get incorporated into the virus particles. *EBioMedicine*. 2014;1(2-3):116-125.

6. Berger C, Day P, Meier G, Zingg W, Bossart W, Nadal D. Dynamics of Epstein-Barr virus DNA levels in serum during EBV-associated disease. *J Med Virol*. 2001;64(4):505-512.

7. Fonteneau JF, Larsson M, Somersan S, et al. Generation of high quantities of viral and tumor-specific human $CD4^+$ and $CD8^+$ T-cell clones using peptide pulsed mature dendritic cells. *J Immunol Methods*. 2001;258(1-2):111-126.

8. Murer A, McHugh D, Caduff N, et al. EBV persistence without its EBNA3A and 3C oncogenes in vivo. *PLoS Pathog*. 2018;14(4):e1007039.

9. McHugh D, Caduff N, Barros MHM, et al. Persistent KSHV infection increases EBV-associated tumor formation in vivo via enhanced EBV lytic gene expression. *Cell Host & Microbe*. 2017;22(1):61-73.

10. Tierney RJ, Shannon-Lowe CD, Fitzsimmons L, Bell AI, Rowe M. Unexpected patterns of Epstein-Barr virus transcription revealed by a high throughput PCR array for absolute quantification of viral mRNA. *Virology*. 2015;474:117-130.

11. Bell AI, Groves K, Kelly GL, et al. Analysis of Epstein-Barr virus latent gene expression in endemic Burkitt's lymphoma and nasopharyngeal carcinoma tumour cells by using quantitative real-time PCR assays. *J Gen Virol*. 2006;87(Pt 10):2885-2890.

12. Nowicka M, Krieg C, Crowell HL, et al. CyTOF workflow: differential discovery in high-throughput high-dimensional cytometry datasets. *F1000Res*. 2017;6:748.